

# A TOPBP1 Allele Causing Male Infertility Uncouples XY Silencing Dynamics From Sex Body Formation

## Reviewed Preprint

Revised by authors after peer review.



## About eLife's process

**Reviewed preprint version 2**  
January 19, 2024 (this version)

**Reviewed preprint version 1**  
September 11, 2023


**Sent for peer review**  
July 18, 2023

**Posted to preprint server**  
June 1, 2023

Carolline F. R. Ascencio, Jennie R. Sims, Alexis Dziubek, William Comstock, Elizabeth A. Fogarty, Jumana Badar, Raimundo Freire, Andrew Grimson, Robert S. Weiss, Paula E. Cohen , Marcus Smolka 

Department of Molecular Biology and Genetics, Cornell University, United States • Fundación Canaria del Instituto de Investigación Sanitaria de Canarias (FIISC), Unidad de Investigación, Hospital Universitario de Canarias, La Laguna, Santa Cruz de Tenerife, Spain • Instituto de Tecnologías Biomédicas, Universidad de La Laguna, 38200 La Laguna, Spain • Universidad Fernando Pessoa Canarias, Las Palmas de Gran Canaria, Spain • Department of Biomedical Sciences, Cornell University, United States

 [https://en.wikipedia.org/wiki/Open\\_access](https://en.wikipedia.org/wiki/Open_access)

 Copyright information

## Abstract

Meiotic sex chromosome inactivation (MSCI) is a critical feature of meiotic prophase I progression in males. While the ATR kinase and its activator TOPBP1 are key drivers of MSCI within the specialized sex body (SB) domain of the nucleus, how they promote silencing remains unclear given their multifaceted meiotic functions that also include DNA repair, chromosome synapsis and SB formation. Here we report a novel mutant mouse harboring mutations in the TOPBP1-BRCT5 domain. *Topbp1*<sup>B5/B5</sup> males are infertile, with impaired MSCI despite displaying grossly normal events of early prophase I, including synapsis and SB formation. Specific ATR-dependent events are disrupted including phosphorylation and localization of the RNA:DNA helicase Senataxin. *Topbp1*<sup>B5/B5</sup> spermatocytes initiate, but cannot maintain ongoing, MSCI. These findings reveal a non-canonical role for the ATR-TOPBP1 signaling axis in MSCI dynamics at advanced stages in pachynema and establish the first mouse mutant that separates ATR signaling and MSCI from SB formation.

### eLife assessment

This **important** study reports a new mutant mouse line with compromised function of a DNA damage response protein. The evidence supporting the conclusion that the mutants display defective maintenance of meiotic sex chromosome inactivation is **solid**. This work is of interest to biomedical researchers working on meiosis and meiotic sex chromosome inactivation.

## Introduction

During Prophase I, the SPO11 topoisomerase-like enzyme and its cofactors induce programmed DNA double-strand breaks (DSBs) that are then recognized by the DNA damage response (DDR) machinery to promote recombination between homologous chromosomes (Handel and Schimenti, 2010; Joshi et al., 2015; Keeney et al., 1997; Subramanian and Hochwagen, 2014). Proper chromosome synapsis achieved through the formation of the proteinaceous synaptonemal complex, together with homologous recombination (HR)-mediated DNA repair (Pereira et al., 2020) are critical for the formation of crossovers that ensure the correct segregation of chromosomes and the formation of healthy and genetically diverse haploid gametes (Gray and Cohen, 2016). Chromosomes that fail to synapse as prophase I progresses trigger a process referred to as meiotic silencing of unsynapsed chromatin (MSUC) (Abe et al., 2020; Burgoyne et al., 2009; Turner, 2015; Turner et al., 2006) to silence genes at unsynapsed regions. In the heterogametic sex (male mammals), the X and Y chromosomes pose a unique challenge for meiotic progression since they bear homology only at the pseudoautosomal region (PAR). The non-homologous arms of the sex chromosomes remain unsynapsed and must therefore undergo a sex-chromosome specific manifestation of MSUC, termed meiotic sex-chromosome inactivation (MSCI) (Alavattam et al., 2018; Royo et al., 2010; Turner, 2007; Turner et al., 2006). MSCI is critical for normal prophase I progression through two complementary mechanisms, the silencing of toxic Y-linked genes, such as *Zfy1* and *Zfy2*, that enforce the pachytene checkpoint (Royo et al., 2010; Vernet et al., 2016) and through the accumulation of the DDR machinery at the X and Y chromosomes, away from the autosomes, during early pachynema (Abe et al., 2020).

The apical serine-threonine kinase Ataxia Telangiectasia mutated and Rad-3 related (ATR), is a master regulator of DNA repair, checkpoints and silencing during prophase I in spermatocytes. In response to DSBs and asynapsis, ATR activation promotes a range of downstream effects, including recombinational DNA repair, crossing over, chromosome synapsis, cell cycle arrest and potentially apoptosis (Abe et al., 2022; Pacheco et al., 2018; Pereira et al., 2020; Royo et al., 2013; Widger et al., 2018). During leptotema and zygotema, shortly after DSB formation, ATR and its cofactor ATRIP are recruited to RPA-coated regions of single strand DNA (ssDNA) that accumulate upon 5'-3' resection of both ends of DSBs (Cimprich and Cortez, 2008; Fanning et al., 2006). ATR activation requires recruitment of TOPBP1 (topoisomerase 2 binding protein 1), a multi-BRCT (BRCA C-terminus motif) domain protein that stimulates ATR kinase activity through its ATR-activation domain (AAD) (Cimprich and Cortez, 2008; Kumagai et al., 2006; Mordes et al., 2008; Zhou et al., 2013). In addition to activating ATR, TOPBP1 also serves as a scaffold for a range of DDR factors, interacting with, and often recruiting them via its multiple BRCT domains (Bigot et al., 2019; Blackford et al., 2015; Cescutti et al., 2010; Delacroix et al., 2007; Leimbacher et al., 2019; Leung et al., 2011; Liu et al., 2017; Pereira et al., 2022). TOPBP1 is composed of nine BRCT domains, which are protein-interacting modules that typically recognize phosphorylated motifs (Liu et al., 2017; Manke et al., 2003; Rodriguez et al., 2003). Through the recognition of phosphoproteins, TOPBP1 is able to assemble multisubunit complexes to promote discrete pathways (Bigot et al., 2019; Blackford et al., 2015; Cescutti et al., 2010; Delacroix et al., 2007; ElInati et al., 2017; Jeon et al., 2019; Leimbacher et al., 2019; Leung et al., 2011; Liu et al., 2017; Pereira et al., 2022, 2020; Perera et al., 2004). TOPBP1 interacts with the C-terminal tail of RAD9, a component of the 9-1-1 PCNA-like clamp that is loaded at 5' recessed junctions adjacent to DSBs (Parrilla-Castellar et al., 2004). The 9-1-1-TOPBP1 complex is essential for canonical ATR signaling during prophase I (ElInati et al., 2017; Jeon et al., 2019; Perera et al., 2004). The interaction of proteins with TOPBP1 may facilitate their phosphorylation by ATR, suggesting a role for TOPBP1 in the control of ATR substrate selection.

As cells progress from zygotema into pachynema, ATR and TOPBP1 localize to the unsynapsed axes of the X and Y chromosomes (Broering et al., 2014; Moens et al., 1999; Reini et al., 2004), leading to phosphorylation of the histone variant H2AX on serine 139 (γH2AX), a major hallmark of MSCI (Royo et al., 2013; Widger et al., 2018). During establishment of MSCI, a

phase separated structure termed the sex body is formed (Monesi, 1965 [↗](#); Solari, 1974 [↗](#); Xu and Qiao, 2021 [↗](#)), allowing the confinement of ATR signaling, DDR factors and silencing to the X and Y (Abe et al., 2020 [↗](#); Turner, 2007 [↗](#)) as part of a checkpoint that may induce cell death if DDR proteins aberrantly accumulate and remain on autosomes (Abe et al., 2020 [↗](#)). Recruitment of ATR and TOPBP1 to unsynapsed regions of the XY requires a distinct set of factors compared to their mode of recruitment to autosomal DSB sites mentioned above, and involves factors such as BRCA1 and HORMAD (Shin et al., 2010 [↗](#); Turner et al., 2004 [↗](#)). Activated ATR phosphorylates H2AX at the unsynapsed cores of the X and Y chromosomes, a signaling that is propagated to chromatin loops of the X and Y, via a feed-forward process mediated by recruitment of the MDC1 adaptor, which further recruits and mobilizes additional TOPBP1-ATR complexes, therefore spreading ATR signaling to promote the broad chromosome-wide silencing required for MSCI (Ichijima et al., 2011 [↗](#)). It has also been proposed that the initiation of MSCI accumulates DDR proteins from autosomes to the X and Y chromosomes to prevent excessive DDR signaling at autosomes from activating cellular checkpoints that can stop meiotic progression (Abe et al., 2020 [↗](#)).

Despite mounting evidence pointing to the importance of ATR and TOPBP1 for MSCI, the precise mechanisms by which they promote sex body formation and XY silencing remain unknown. Moreover, it remains unclear how these two processes are spatiotemporally coordinated and how ATR and TOPBP1 mediate such coordination. Since both proteins are essential for organismal viability (Brown and Baltimore, 2000 [↗](#); De Klein et al., 2000 [↗](#); Jeon et al., 2011 [↗](#); O'Driscoll, 2009 [↗](#); O'Driscoll et al., 2007 [↗](#); Yamane et al., 2002 [↗](#); Zhou et al., 2013 [↗](#)), conditional knockouts (ElInati et al., 2017 [↗](#); Royo et al., 2013 [↗](#); Widger et al., 2018 [↗](#)) or hypomorphic (Pacheco et al., 2018 [↗](#)) models have been used to explore their roles during prophase I in spermatocytes. However, given the strong pleiotropic effects in these models, especially in DSB repair, synapsis, MSCI and sex body formation, it is difficult to dissect the distinct molecular mechanisms involved, and to untangle direct versus indirect effects. Here we present a separation-of-function mouse mutant that deconvolutes TOPBP1-dependent ATR signaling in male meiosis. We generated mice bearing multiple mutations in BRCT-domain 5 (*Topbp1*<sup>B5/B5</sup> mice) that are viable and grossly indistinguishable from wild-type littermates; yet, the males are sterile, having reduced testes size, reduced seminiferous tubule cellularity, and a complete loss of sperm. Strikingly, while *Topbp1*<sup>B5/B5</sup> spermatocytes fail to progress into diplotene, they display largely normal chromosome synapsis, sex body formation, recruitment of DDR proteins to the X and Y, and DNA repair during prophase I, in sharp contrast to previous models of TOPBP1 or ATR impairment (ElInati et al., 2017 [↗](#); Widger et al., 2018 [↗](#)). Single-cell RNA sequencing data showed that while MSCI is initiated in *Topbp1*<sup>B5/B5</sup>, the dynamics of silencing progression and reinforcement is defective, which is accompanied by a defect in the localization of the RNA:DNA helicase Senataxin to chromatin loops of the XY chromosomes. We propose that the *Topbp1*<sup>B5/B5</sup> is a separation of function mutant that allows the untangling of XY silencing from sex body formation and DDR recruitment to the XY, representing a unique model to study the establishment, maintenance, reinforcement and progression of MSCI.

## Results

### A TOPBP1 mutant separating its role in fertility from organismal viability

*Topbp1* knockout mice exhibit strong defects early in embryonic development, reaching blastocyst stage but not progressing beyond E.8, with embryos likely dying at the preimplantation stage (Jeon et al., 2011 [↗](#)). In the context of meiosis, conditional knockout of *Topbp1* in spermatocytes leads to pleiotropic effects, including defects in chromosome synapsis, impaired recruitment of DDR factors to XY chromosomes, defects in condensation of the XY chromosomes, abnormal formation of the sex body, lack of γH2AX spreading to chromatin loops, all of which contribute to a strong MSCI defect as indicated by the complete absence of downstream markers of MSCI, such as USP7,

H3K9me3, poly-ubiquitination and sumoylation (ElInati et al., 2017; Pereira et al., 2020). The availability of a separation of function mutant for *Topbp1* is therefore needed to dissect its distinct roles in development, organismal maintenance, and multiple meiotic processes such as DNA repair, silencing and sex body formation. To generate a separation of function mouse model, we inserted eight charge reversal point mutations in BRCT domain 5 of TOPBP1 (hereafter referred to as *Topbp1*<sup>B5/B5</sup>) CRISPR/Cas9 (Figure 1A). After validating the point mutations through Sanger sequencing, (Supplemental Figure 1), we found that *Topbp1*<sup>B5/B5</sup> mice were viable, with no difference in body mass when compared to WT littermates (Figures 1B and 1C), and no sensitivity to Ionizing Radiation (IR) (Figures 1D). Strikingly, *Topbp1*<sup>B5/B5</sup> mice displayed male-specific infertility (Figure 1E), with a three-fold reduction in testis size (Figures 1F and 1G) and complete lack of spermatozoa (Figure 1H). H&E-stained histological testis sections revealed mainly spermatogonia and spermatocytes within the seminiferous epithelium (Figure 1I) together with an increased number of TUNEL-positive spermatocytes in seminiferous tubules (Figure 1J and 1K). Cytological evaluation of surface-spread spermatocytes from *Topbp1*<sup>B5/B5</sup> revealed the presence of meiotic prophase I stages from leptotema to pachynema but a total absence of diplotema-staged spermatocytes (Figure 1L). Moreover, the staining of the synaptonemal complex proteins SYCP1 and SYCP3 revealed normal pachytene entry and no gross defects in chromosome synapsis, distinct from previous models of ATR and TOPBP1 conditional depletion (ElInati et al., 2017; Widger et al., 2018). Furthermore, unlike reported DDR CKO (conditional knockouts) models such as *Rad1* and *Brca1* (Abe et al., 2020; Broering et al., 2014; Pereira et al., 2022), *Topbp1*<sup>B5/B5</sup> pachytene spermatocytes reach mid-pachynema, as demonstrated by the accumulation of signal for H1t (Inselman et al., 2003) (Figure 1L).

### *Topbp1*<sup>B5/B5</sup> MEFs display no detectable DDR defects

To assess the possibility of a somatic phenotype we derived mouse embryonic fibroblasts (MEFs) from *Topbp1*<sup>B5/B5</sup> and wild-type littermates at embryonic day E13.5. Consistent with the observed organismal viability and the lack of IR sensitivity, *Topbp1*<sup>B5/B5</sup> MEFs showed no sensitivity to hydroxyurea (replication stress) or phleomycin (DSBs) in a long-term cell survival assay (Figure 2A-D and Supplemental Figure 2). Genotoxic stress activates the apical kinases ATR, ATM and DNA-PKcs (Blackford and Jackson, 2017; Falck et al., 2005; Maréchal and Zou, 2013) to trigger a signaling cascade that promotes DNA repair and cell cycle arrest via activation of the downstream checkpoint kinases CHK1 and CHK2 (Hartwell and Kastan, 1994; Lanz et al., 2019; Shiloh, 2003). Similar to wild-type MEFs, *Topbp1*<sup>B5/B5</sup> MEFs were able to activate DDR signaling responses when challenged with hydroxyurea and phleomycin as demonstrated by the induction of established damage-induced phosphorylation of CHK1, CHK2, RPA2 and KAP1 (Figure 2E). In addition, *Topbp1*<sup>B5/B5</sup> MEFs were able to recruit MDC1 to γH2AX-marked DSB foci when subjected to IR (Figure 2F) and showed no increased number of micronuclei, a known marker of defective DNA damage responses (Kwon et al., 2020), when compared to *Topbp1*<sup>+/+</sup> MEFs (Supplemental Figure 3A-B).

The BRCT-5 domain of TOPBP1 is known to interact with the DDR factors 53BP1 (Bigot et al., 2019; Cescutti et al., 2010; Liu et al., 2017), MDC1 (Wang et al., 2011) and BLM (Blackford et al., 2015) through phospho-protein binding modules. To investigate which, if any, of these interactions are disrupted upon mutating the eight BRCT5 residues, we ectopically expressed Flag-TOPBP1-WT or Flag-TOPBP1-B5 in HEK293T cells. We found that binding of Flag-TOPBP1-B5 to BLM and 53BP1 was impaired, as expected (Supplemental Figure 4A-B). Moreover, we noticed a 2-fold reduction in protein levels of Flag-TOPBP1-B5 compared to Flag-TOPBP1-WT, which could be explained by the loss of interaction with BLM (that was proposed to lead to protein stabilization (Balbo Pogliano et al., 2022; Wang et al., 2013)), or by protein misfolding caused by the 8 E/D mutations. In addition, the reduction in protein levels was detected on MEFs (Supplemental Figure 5). In either case, the results presented here show that the TOPBP1-B5 mutant offers a unique model to separate roles of TOPBP1 in male meiosis from the canonical DDR functions of TOPBP1 in somatic cells.



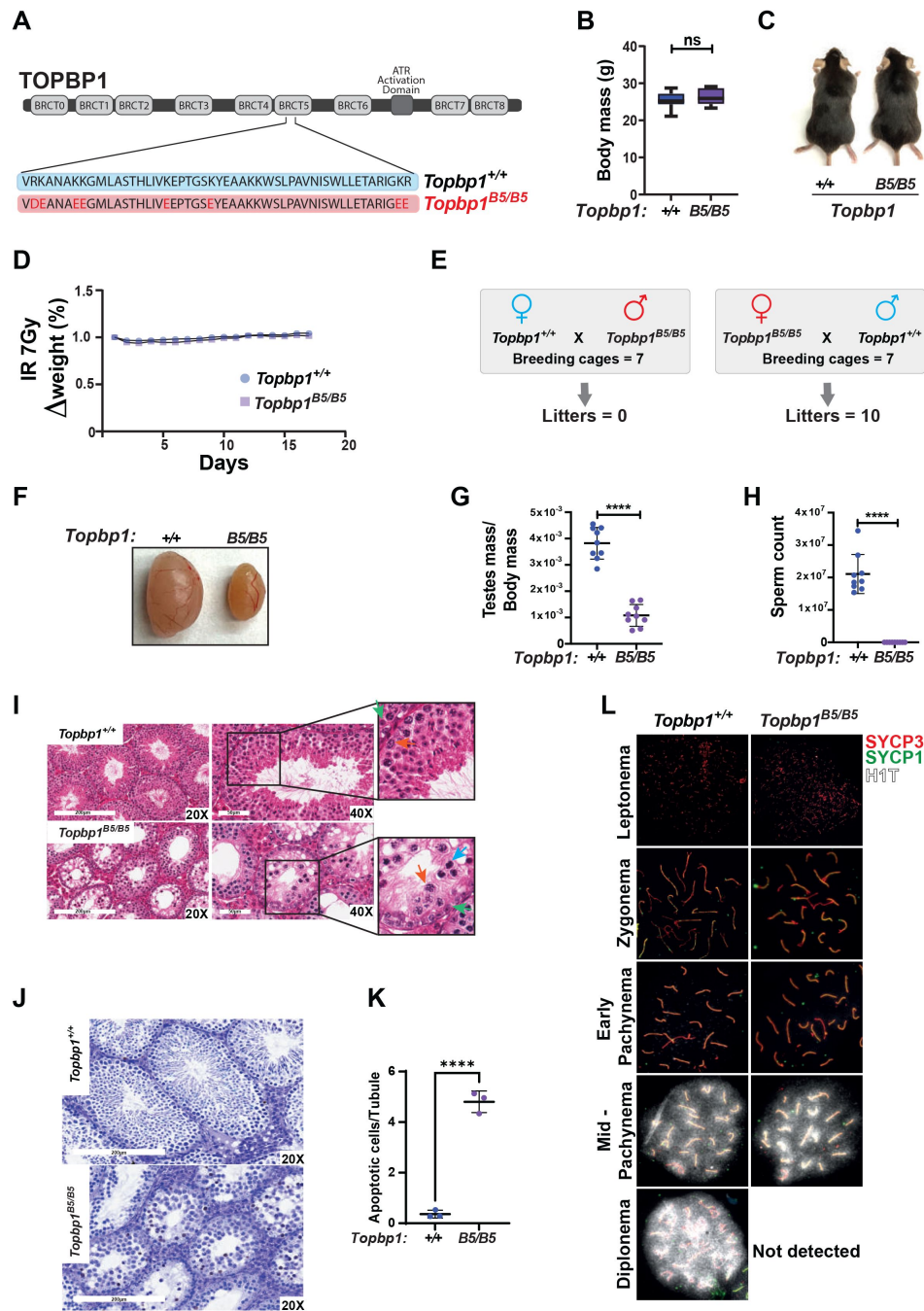


**Figure 1.**

### A new TOPBP1 mutant separating its role in fertility from organismal viability.

A) Schematic showing mutations in the *Topbp1* B5 allele. B) Body mass (*Topbp1*<sup>+/+</sup> Mean = 25.26, SD = 2.38; *Topbp1*<sup>B5/B5</sup> Mean = 26.43, SD = 2.28, n = 9) and C) appearance of *Topbp1*<sup>B5/B5</sup> and *Topbp1*<sup>+/+</sup> littermate mice. D) Effect of full body IR (7 Gy) on changes in body mass of *Topbp1*<sup>B5/B5</sup> and *Topbp1*<sup>+/+</sup> littermate mice. E) Breeding scheme and resulting litters. F) and G) Comparison of testes size (*Topbp1*<sup>+/+</sup> Mean = 0.038, SD = 0.006; *Topbp1*<sup>B5/B5</sup> Mean = 0.011, SD = 0.004, n = 9), and H) sperm count, of *Topbp1*<sup>B5/B5</sup> and *Topbp1*<sup>+/+</sup> littermate mice (*Topbp1*<sup>+/+</sup> Mean =  $2.1 \times 10^7$ , SD =  $6 \times 10^6$ ; *Topbp1*<sup>B5/B5</sup> Mean = 0.0, SD = 0.0, n = 9). I) H&E-stained histological testes sections displaying loss of cellularity in *Topbp1*<sup>B5/B5</sup>. Green arrow = spermatogonia, Red arrow = healthy spermatocyte, Blue arrow = dying spermatocyte. J) and K) TUNEL assay performed on histological testes sections (*Topbp1*<sup>+/+</sup> Mean = 0.36, SD = 0.15; *Topbp1*<sup>B5/B5</sup> Mean = 4.80, SD = 0.43, n = 3). L) Meiotic spreads stained for SYCP3, SYCP1 and H1t. \*\*\*\* = p < 0.0001, n = number of mice. p-Values were calculated using unpaired t-test.

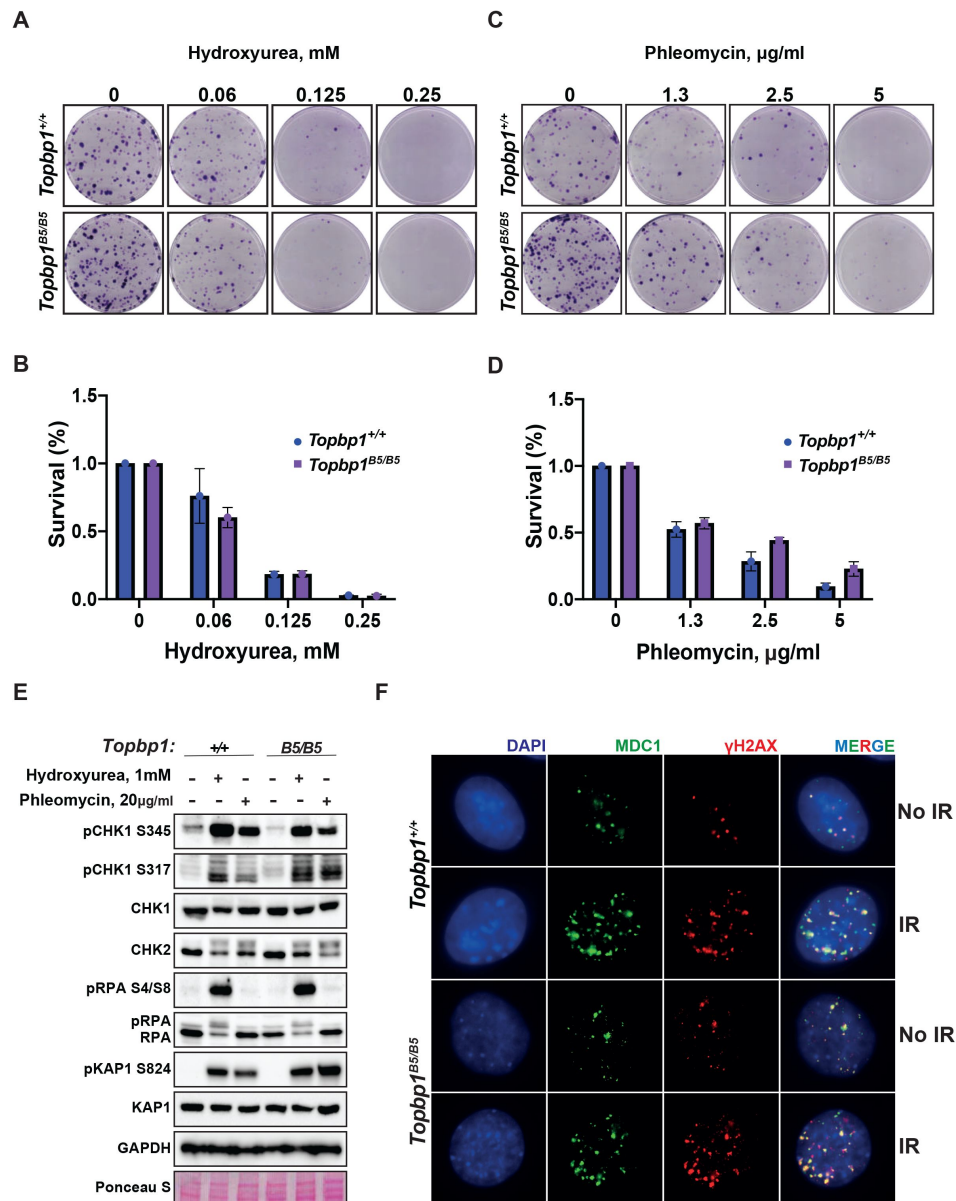


**Figure 2.**

***Topbp1*<sup>B5/B5</sup> MEFs display no detectable DDR defects.**

A) MEFs obtained from littermate mice of indicated genotypes were subjected to clonogenic survival assay in the indicated concentrations of hydroxyurea, or C) phleomycin. B) and D) Quantification of clonogenic survival assays from A and C, respectively, performed in biological and experimental triplicates. D) Western blot for indicated DDR markers in MEFs obtained from *Topbp1*<sup>B5/B5</sup> and *Topbp1*<sup>+/+</sup> littermate mice. The data from MEFs were performed using littermate pairs and validated using a second pair of *Topbp1*<sup>B5/B5</sup> and *Topbp1*<sup>+/+</sup> littermate mice. E) Immunofluorescence of MDC1 and phosphoH2AX\_S139-stained nuclei from *Topbp1*<sup>B5/B5</sup> and *Topbp1*<sup>+/+</sup> MEFs treated with IR (7 Gy).

## ***Topbp1*<sup>B5/B5</sup> spermatocytes display normal markers of canonical ATR signaling, chromosome synapsis, DNA repair, sex body formation, and DDR protein localization at the X and Y**

TOPBP1 and ATR play multiple roles in spermatocytes during prophase I. Mice conditionally depleted for TOPBP1 (ElInati et al., 2017 [↗](#)) or ATR (Royo et al., 2013 [↗](#); Widger et al., 2018 [↗](#)) display severe defects in chromosome synapsis, DNA DSB repair, sex body formation and MSCI, as well as impaired recruitment of DDR factors to the XY (Pereira et al., 2020 [↗](#)). Strikingly, analysis of *Topbp1*<sup>B5/B5</sup> spermatocytes via meiotic spreads revealed normal repair of DNA DSBs, with γH2AX staining grossly unchanged at pachynema, being confined only to the XY chromosomes and being excluded from the autosomes (Figure 3A-B [↗](#)). RAD51 localized only to the X and Y chromosomes during mid-pachytene (Figure 3C-D [↗](#)), indicating normal DSB repair at the autosomes. We were unable to detect chromosome synapsis abnormalities in *Topbp1*<sup>B5/B5</sup> spermatocytes, as *Topbp1*<sup>B5/B5</sup> mutant spermatocytes transit from zygotene into pachytene with normal patterns of HORMAD1 and HORMAD2 localization (Supplemental Figure 6A-B) and with SYCP1 overlapping with SYCP3 on chromosome cores from all autosomal chromosomes during pachynema (Figures 1L [↗](#) and 3E [↗](#)). Since ATR orthologs regulate crossing over in budding yeast (Subramanian and Hochwagen, 2014 [↗](#)) and in *Drosophila melanogaster* (Carpenter, 1979 [↗](#)), we also investigated the localization of factors involved in regulating DNA crossovers, including MLH1 and MLH3. In *Topbp1*<sup>B5/B5</sup> spermatocytes, while the number of MLH1 foci were significantly increased, the number of MLH3 foci did not differ significantly (Supplemental Figure 7A and 7B). Due to the lack of diplotene cells, and any other stage after pachynema, we were not able to test whether *Topbp1*<sup>B5/B5</sup> display defects in crossing over.

The sex body appeared normal in its shape and was normally formed in *Topbp1*<sup>B5/B5</sup> spermatocytes (Figures 3A [↗](#) and Supplemental Figures 8 and 9A), exhibiting only subtle defects/delays in the spreading of the γH2AX signal on the PAR and pericentromeric regions (Supplemental Figure 9B- G). Although the defect was subtle in its severity, it accounted for 56% of all γH2AX-stained mid- pachytene cells. Importantly, TOPBP1 was normally localized to X and Y chromosomes during prophase I (Supplemental Figure 10 and Figure 3F-H [↗](#)). Similarly, localization of the TOPBP1 interactors ATR, BRCA1, MDC1, and 53BP1 in *Topbp1*<sup>B5/B5</sup> spermatocytes spreads was also indistinguishable from that observed in *Topbp1*<sup>+/+</sup> spermatocytes (Figures 4A-F [↗](#) and Supplemental Figures 11). Markers of ATR signaling were also mostly normal, as measured by its canonical targets pMDC1 T4 (Supplemental Figure 6C-D), pCHK1 S345 (Supplemental Figure 6E-F), and pHORMAD2 (Supplemental Figure 6G-H). Notably, we did observe that phosphorylation of CHK1 on S317 was significantly decreased in *Topbp1*<sup>B5/B5</sup> when compared to *Topbp1*<sup>+/+</sup> spermatocytes (Figure 4G-H [↗](#)). However, since *Chk1* CKO spermatocytes complete prophase I and differentiate into spermatozoa, with only minor defects such a delay in the removal of γH2AX from autosomes (Abe et al., 2018 [↗](#)), the observed defect in Chk1 S317 phosphorylation is unlikely to be the cause of the infertility observed in *Topbp1* B5 mutants. Overall, as summarized in Figure 4I [↗](#), *Topbp1*<sup>B5/B5</sup> spermatocytes appear to progress normally through early stages of prophase I up until the end of pachynema as demonstrated by largely normal localization of markers for DNA repair, chromosome synapsis and ATR signaling. These findings are surprising because the lack of sex body formation, synapsis defects or unrepaired DSBs, which are the expected causes of the drastic loss of diplotene cells and the lack of spermatozoa, were not observed.

## **Defective phosphorylation and XY localization of the RNA:DNA helicase SETX in *Topbp1*<sup>B5/B5</sup> spermatocytes**

With the exception of CHK1 phosphorylation at serine 317, the analysis of other canonical markers of ATR signaling on meiotic prophase I spreads did not reveal obvious defects in their distribution or intensity at the XY body (Figure 4G-H [↗](#) and Supplemental Figure 6C-H). Since altered CHK1

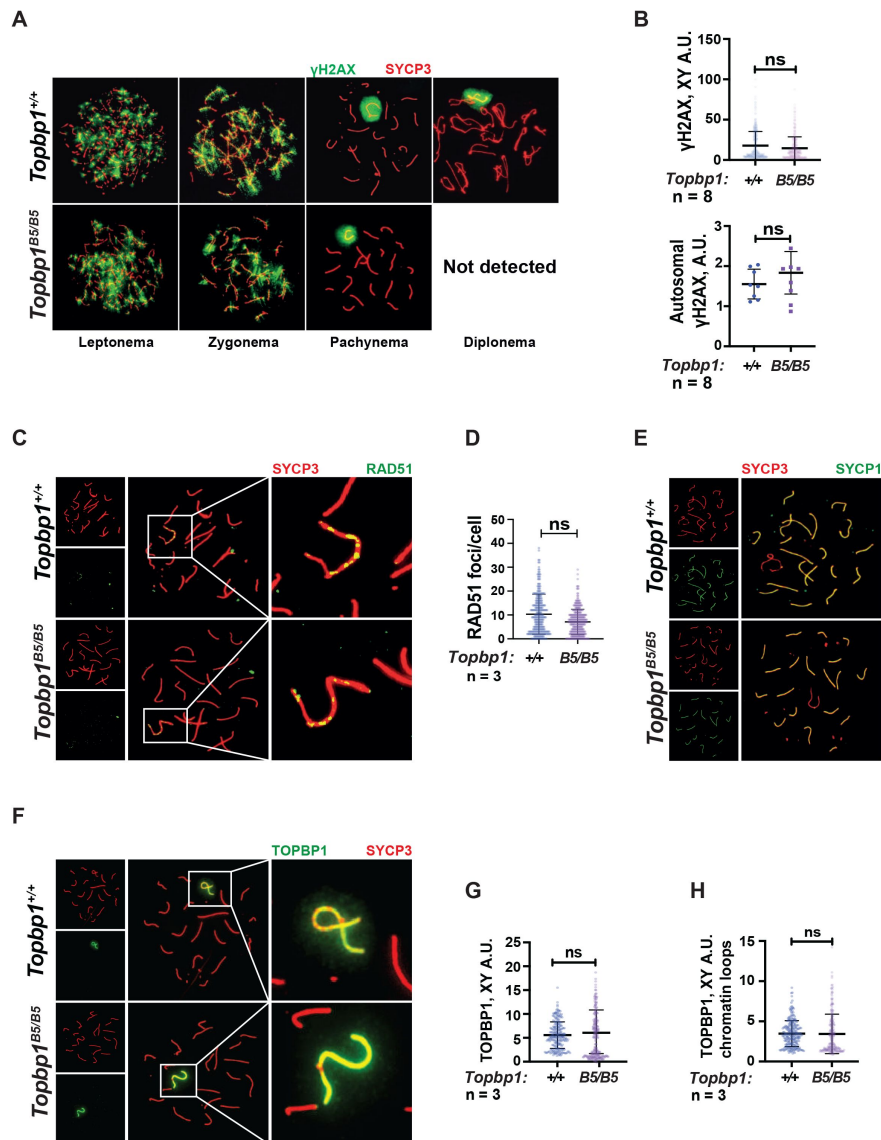


**Figure 3.**

### Markers of DNA repair, synapsis, sex body formation and TOPBP1 localization are mostly normal in *Topbp1*<sup>B5/B5</sup> spermatocytes.

A) Meiotic spreads showing *Topbp1*<sup>+/+</sup> and *Topbp1*<sup>B5/B5</sup> spermatocytes stained with SYCP3 and yH2AX, prepared as described in methods. B) Quantification of yH2AX-stained pachytene spreads, upper graph XY body (each dot represents one pachytene cell measured; *Topbp1*<sup>+/+</sup> number of cells = 386, number of mice = 8; *Topbp1*<sup>B5/B5</sup> number of cells = 410, number of mice = 8; p-value = 0.3063), bottom graph autosomal chromosomes (each dot represents the average of signal from all autosomes in each mouse, *Topbp1*<sup>+/+</sup> number of cells = 160, number of mice = 8; *Topbp1*<sup>B5/B5</sup> number of cells = 161, number of mice = 8; p-value = 0.5081). C) Meiotic spreads showing *Topbp1*<sup>+/+</sup> and *Topbp1*<sup>B5/B5</sup> pachytene spermatocytes stained with SYCP3 and RAD51. D) Quantification of RAD51 foci/cell of mid-pachytene meiotic spreads (each dot represents one pachytene cell measured; *Topbp1*<sup>+/+</sup> number of cells = 149, number of mice = 3; *Topbp1*<sup>B5/B5</sup> number of cells = 183, number of mice = 3; p-value = 0.2174). E) Meiotic spreads showing *Topbp1*<sup>+/+</sup> and *Topbp1*<sup>B5/B5</sup> pachytene spermatocytes stained with SYCP3 and SYCP1. F) Meiotic spreads showing *Topbp1*<sup>+/+</sup> and *Topbp1*<sup>B5/B5</sup> pachytene spermatocytes stained with SYCP3 and TOPBP1. G) Quantification of TOPBP1 on X and Y chromosome cores from F (each dot represents one pachytene cell measured; *Topbp1*<sup>+/+</sup> number of cells = 246, number of mice = 3; *Topbp1*<sup>B5/B5</sup> number of cells = 233, number of mice = 3; p-value = 0.8546). H) Quantification of TOPBP1 on X and Y chromatin loops from F (each dot represents one pachytene cell measured; *Topbp1*<sup>+/+</sup> number of cells = 246, number of mice = 3; *Topbp1*<sup>B5/B5</sup> number of cells = 233, number of mice = 3; p-value = 0.6755). n = number of mice. p-Values were calculated using a linear mixed effect model (see Materials and Methods for details).



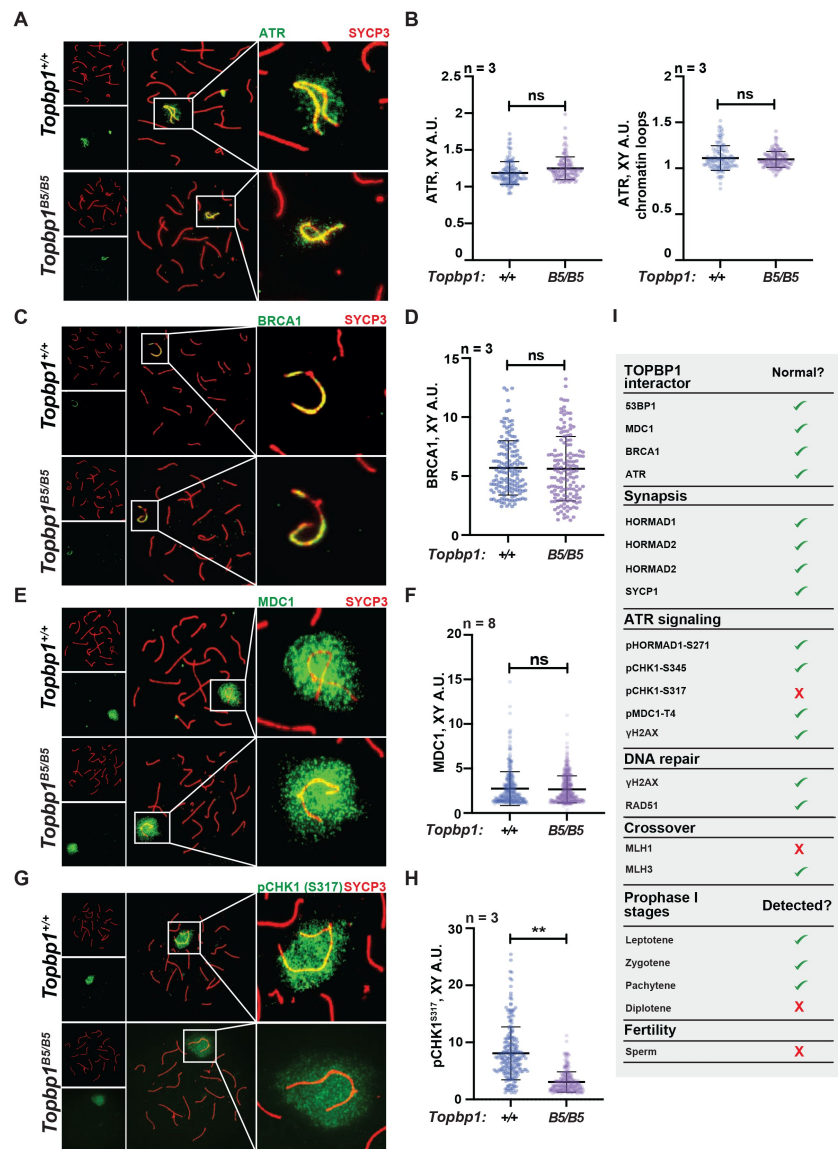


**Figure 4.**

### *Topbp1*<sup>B5/B5</sup> spermatocytes display normal localization of ATR, BRCA1, MDC1 and pMDC1-T4.

A) Meiotic spreads showing *Topbp1*<sup>+/+</sup> and *Topbp1*<sup>B5/B5</sup> pachytene spermatocytes stained with SYCP3 and ATR. B) Quantification of ATR in pachytene spreads from A. Left: ATR on X and Y chromosome cores (each dot represents one pachytene cell measured; *Topbp1*<sup>+/+</sup> number of cells = 127, number of mice = 3; *Topbp1*<sup>B5/B5</sup> number of cells = 127, number of mice = 3; p-value = 0.4068). Right: ATR on X and Y chromatin loops (each dot represents one pachytene cell measured; *Topbp1*<sup>+/+</sup> number of cells = 127, number of mice = 3; *Topbp1*<sup>B5/B5</sup> number of cells = 127, number of mice = 3; p-value = 0.9396). C) Meiotic spreads showing *Topbp1*<sup>+/+</sup> and *Topbp1*<sup>B5/B5</sup> pachytene spermatocytes stained with SYCP3 and BRCA1. D) Quantification of BRCA1 in pachytene spreads from C (each dot represents one pachytene cell measured; *Topbp1*<sup>+/+</sup> number of cells = 152, number of mice = 3; *Topbp1*<sup>B5/B5</sup> number of cells = 140, number of mice = 3; p-value = 0.6509). E) Meiotic spreads showing *Topbp1*<sup>+/+</sup> and *Topbp1*<sup>B5/B5</sup> pachytene spermatocytes stained with SYCP3 and MDC1. F) Quantification of MDC1 in pachytene spreads from E (each dot represents one pachytene cell measured; *Topbp1*<sup>+/+</sup> number of cells = 696, number of mice = 8; *Topbp1*<sup>B5/B5</sup> number of cells = 988, number of mice = 8; p-value = 0.3603). G) Meiotic spreads showing *Topbp1*<sup>+/+</sup> and *Topbp1*<sup>B5/B5</sup> pachytene spermatocytes stained with SYCP3 and pCHK1-S317. H) Quantification of pCHK1-S317 in pachytene spreads from G (each dot represents one pachytene cell measured; *Topbp1*<sup>+/+</sup> number of cells = 223, number of mice = 3; *Topbp1*<sup>B5/B5</sup> number of cells = 254, number of mice = 3; \*\*p-value = 0.0023). p-Values were calculated using a linear mixed effect model (see Materials and Methods for details). I) Table summarizing the normal or disrupted events during male fertility accessed in *Topbp1*<sup>B5/B5</sup>. n = number of mice.



regulation is unlikely to be the cause of the drastic defect in meiotic progression observed in *Topbp1*<sup>B5/B5</sup> males, we investigated whether other branches of ATR signaling were altered in *Topbp1*<sup>B5/B5</sup> spermatocytes by performing unbiased quantitative phosphoproteomics based on TMT (Tandem Mass Tag (Thompson et al., 2003 [DOI](#))) labeling of whole testes. Following a similar approach previously used by our group (Sims et al., 2022 [DOI](#)), we analyzed the phosphoproteome of *Topbp1*<sup>B5/B5</sup> and *Topbp1*<sup>+/+</sup> testes, and then compared the results to our previously reported dataset comparing the phosphoproteome of testes from mice treated with vehicle or the ATR inhibitor AZ20 (Sims et al., 2022 [DOI](#)) (**Figure 5A** [DOI](#)). The resulting plot revealed that ATR-dependent signaling is not drastically impaired in *Topbp1*<sup>B5/B5</sup> testes, as opposed to the marked impairment of ATR signaling previously observed in testes of *Rad1* CKO mice (Sims et al., 2022 [DOI](#)). This finding is in agreement with the results from meiotic spreads of *Topbp1*<sup>B5/B5</sup> showing no detectable defects in canonical markers of ATR signaling described above. Nonetheless, our phosphoproteomic analysis did reveal phosphorylation sites mildly disrupted in *Topbp1*<sup>B5/B5</sup> testes compared to *Topbp1*<sup>+/+</sup> testes. In particular, we noticed that several phosphorylation sites in the RNA:DNA helicase, Senataxin (SETX) (Cohen et al., 2018 [DOI](#)), including a phosphorylation in the preferred motif for ATR phosphorylation (S/T-Q), were down-regulated in *Topbp1*<sup>B5/B5</sup> mice (**Figure 5B** [DOI](#)). Interestingly, SETX was previously associated with meiotic ATR functions and found to be indispensable for MSCI (Becherel et al., 2013 [DOI](#); Yeo et al., 2015 [DOI](#)). Moreover, we recently reported that mice treated with the ATR inhibitor AZ20 or lacking *Rad1* display reduced phosphorylation of SETX at S/T-Q site and SETX mislocalization during pachynema (Sims et al., 2022 [DOI](#)). Based on our findings, we propose that TOPBP1 regulates SETX distribution and/or function during meiosis, and that defects in meiotic progression and fertility observed in *Topbp1*<sup>B5/B5</sup> mice might be associated with SETX dysfunction. Consistent with this possibility, we found that pachytene spermatocytes from *Topbp1*<sup>B5/B5</sup> display significantly decreased spreading of SETX to XY chromatin loops while still displayed SETX at the unsynapsed axes of the X and Y chromosomes (**Figures 5C-F** [DOI](#)). Overall, these findings reveal that *Topbp1*<sup>B5/B5</sup> spermatocytes display largely normal progression through mid-pachynema, as demonstrated by normal distribution of a range of markers of meiotic progression, including canonical markers of ATR signaling. However, in-depth phosphoproteomic and imaging analyses identify specific defects in the regulation of SETX, a target of ATR signaling during prophase I (Pereira et al., 2022 [DOI](#); Sims et al., 2022 [DOI](#)) and a key factor required for MSCI (Becherel et al., 2013 [DOI](#); Yeo et al., 2015 [DOI](#)).

## ***Topbp1*<sup>B5/B5</sup> spermatocytes initiate MSCI but fail to promote full XY silencing**

During mid-pachynema, spermatocytes that fail to properly silence the X and Y chromosomes arrest and trigger apoptosis-induced cell death (Abe et al., 2020 [DOI](#); Ichijima et al., 2012 [DOI](#); Turner, 2015 [DOI](#), 2007 [DOI](#)). In mice, the MSCI process initiates in leptotene (Lau et al., 2020 [DOI](#)), and during early pachynema key events occur at the XY chromosomes, such as exclusion of RNA polymerase 2 (RNA Pol2), recruitment of DDR proteins and chromatin remodelers and establishment of heterochromatin marks (Abe et al., 2020 [DOI](#); Khalil et al., 2004 [DOI](#)) to maintain the active silencing of the X and Y chromosomes (Abe et al., 2022 [DOI](#)). This process leads to the formation of a membrane-less phase separated structure termed the sex body (Alavattam et al., 2022 [DOI](#); Xu and Qiao, 2021 [DOI](#)).

Spermatocytes from *Topbp1*<sup>B5/B5</sup> males formed a sex body of grossly normal appearance (Supplemental Figure 8), with undisrupted patterns of the sex body markers CHD4, SUMO, and USP7 (Supplemental Figure 12). *Topbp1*<sup>B5/B5</sup> pachytene spermatocytes also display normal patterns of a range of chromatin marks, including H3K9ac, H3K9me3, H3K27ac, H3K36me3, H3K4me3, H4K16ac, H4ac, H2AK116ub, H3K4me1, as well as proper exclusion of RNA Pol2 from the sex body (Supplemental Figures 13-17). Collectively the evidence presented herein shows that *Topbp1*<sup>B5/B5</sup> mutants are able to form grossly normal XY bodies, with proper localization of over 28 markers, the severe loss of diplotene cells and the reduction of SETX at the chromatin loops of

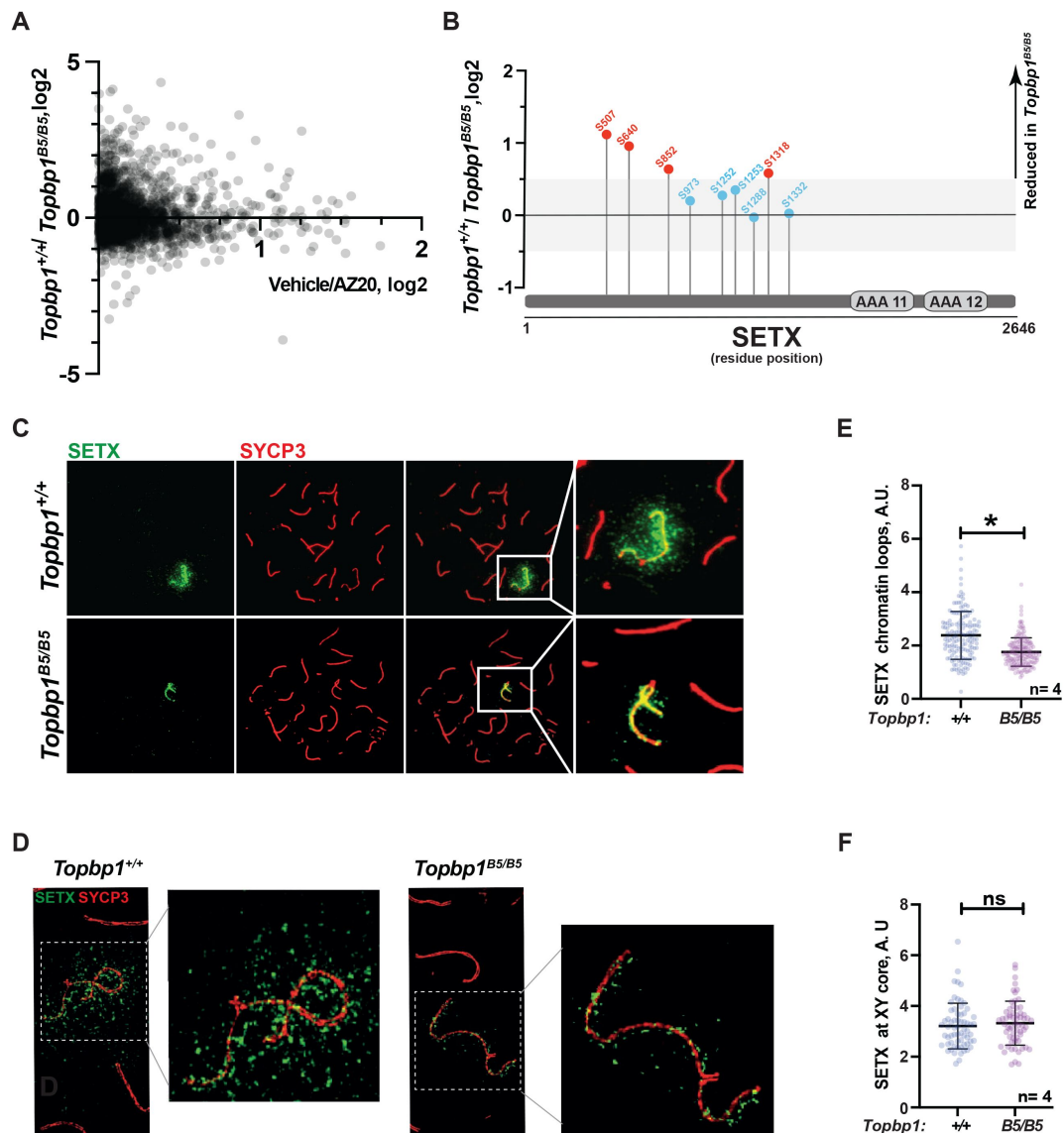


**Figure 5.**

### Defective SETX phosphorylation and localization in *Topbp1*<sup>B5/B5</sup> spermatocytes.

A) Scatter plot of phosphoproteomic datasets corresponding to *Topbp1*<sup>+/+</sup>/*Topbp1*<sup>B5/B5</sup> (Y axis) and *Topbp1*<sup>+/+</sup> (vehicle)/*Topbp1*<sup>+/+</sup> (AZ20) (X axis) from whole testes of mice. B) SETX phosphopeptides identified in the *Topbp1*<sup>+/+</sup>/*Topbp1*<sup>B5/B5</sup> phosphoproteomic experiment shown in A. Red: reduced in *Topbp1*<sup>B5/B5</sup> mutant; Blue: unchanged. C) Meiotic spreads showing pachytene spermatocytes from *Topbp1*<sup>+/+</sup> and *Topbp1*<sup>B5/B5</sup> mice stained with SYCP3 and SETX in regular immunofluorescence. D) 3D-SIM analysis of meiotic spreads described in C. E) Quantification of SETX on X and Y chromatin loops in pachytene spreads from C (each dot represents one pachytene cell measured; *Topbp1*<sup>+/+</sup> number of cells = 152, number of mice = 4; *Topbp1*<sup>B5/B5</sup> number of cells = 174, number of mice = 4; \*p-value = 0.0452). F) Quantification of SETX on X and Y chromosome cores in pachytene spreads from C (each dot represents one pachytene cell measured; *Topbp1*<sup>+/+</sup> number of cells = 152, number of mice = 4; *Topbp1*<sup>B5/B5</sup> number of cells = 174, number of mice = 4; p-value = 0.5987). p-Values were calculated using a linear mixed effect model (see Materials and Methods for details).

the X and Y lead us to speculate that *Topbp1*<sup>B5/B5</sup> spermatocytes may still have a defective MSCI. To investigate potential MSCI defects, we employed single cell RNA sequencing (sc-RNA-seq) in germ cells (**Figure 6A**) using a similar approach recently used to follow spermatogenesis progression and to evaluate MSCI in mammals (Grive et al., 2019; Jung et al., 2019; Lau et al., 2020). Using the 10X platform we performed sc-RNA-seq on a germ cell-enriched population of cells extracted from adult *Topbp1*<sup>+/+</sup> and *Topbp1*<sup>B5/B5</sup> testes (**Figure 6A**). The data were analyzed as previously described (Grive et al., 2019; Lau et al., 2020) using signature genes as markers of different stages in spermatogenesis such as, *Sal4* and *Dmrt1* for spermatogonia, *Dazl* for early spermatocytes, *Id4*, *Sycp3* and *Shcbp1l* for late spermatocytes, *Acrv1* for round spermatids, and *Oaz3* and *Prm2* for elongated spermatids (Supplemental Figures 18 and 19). *Col1a2*, *Acta2*, *Vcam1*, *Lns13*, *laptm5*, *Hbb-bt*, *Ptgds* and *Wt1* were used as markers of somatic cells (Supplemental Figure 20). Analysis of the testicular transcriptome of *Topbp1*<sup>+/+</sup> males revealed 47 sub-clusters of cells covering spermatogonia, spermatocytes, spermatids, and somatic cells (**Figure 6B-D** and Supplemental Figures 21-22). In sharp contrast, analysis of *Topbp1*<sup>B5/B5</sup> germ cell population revealed only somatic, spermatogonia and the initial populations of spermatocytes (**Figure 6D**). This result corroborates the H&E-stained testes histological sections (**Figure 1I**) and meiotic spreads (**Figure 1L**). Importantly, Pearson correlation values from all RNA reads between cell groups separated by cluster and genotype, demonstrated the similarity of spermatocytes from *Topbp1*<sup>+/+</sup> and *Topbp1*<sup>B5/B5</sup> (Supplemental Figure 23). As shown in **Figure 6E**, we were able to monitor the dynamics of X chromosome silencing in the early-stage spermatocytes and compare the results between RNA from *Topbp1*<sup>+/+</sup> and *Topbp1*<sup>B5/B5</sup> males. Strikingly, *Topbp1*<sup>B5/B5</sup> early-stage spermatocytes could initiate MSCI and promote robust, albeit incomplete, X chromosome silencing. Both X and Y chromosomes showed increased gene expression levels in the last spermatocyte stage captured in *Topbp1*<sup>B5/B5</sup> males when compared to RNA from wild type males (**Figure 6E** and Supplemental Figure 24). Moreover, although certain X-genes from *Topbp1*<sup>B5/B5</sup> pachytene cells consistently demonstrated defects in silencing by being expressed in numerous cells, other genes were only expressed in a small number of cells. This highlights the non-uniformity of the MSCI defect in all pachytene cells (Supplemental Figure 24). Notably, while we detected only a minor elevation in the levels of X-linked gene expression in *Topbp1*<sup>B5/B5</sup> spermatogonia when compared to *Topbp1*<sup>+/+</sup>, the expression of X-linked genes at spermatocyte 3 stage was drastically higher in *Topbp1*<sup>B5/B5</sup> males when compared to *Topbp1*<sup>+/+</sup> males. To improve the accuracy of the downstream analysis, the expression levels of X-linked genes were normalized by their respective expression level at the pre-leptotene stage.

MSCI is a dynamic process that involves the accumulation of DDR factors at the X and Y chromosomes as cells enter pachynema (Abe et al., 2022, 2020) as well as the inactivation of specific X and Y genes that lead to cell death if expressed at this stage (the so called “killer genes”) (Royo et al., 2010; Vernet et al., 2016). Similar to previous reports based on mutants or treatments that impaired MSCI (Abe et al., 2022; ElInati et al., 2017; Hirota et al., 2018; Modzelewski et al., 2012; Pereira et al., 2022; Royo et al., 2013; Widger et al., 2018), transcriptomics profiles from *Topbp1*<sup>B5/B5</sup> testicular cells showed an increased number of stage 3 spermatocytes (SP3 - pachytene) expressing the spermatocyte-toxic genes *Zfy1* and *Zfy2* compared to *Topbp1*<sup>+/+</sup> (Supplemental Figures 25-26). Other genes typically used to illustrate MSCI defects, such as *Kdm6a*, *lamp2*, *Zfx*, *Uba1y* and *Rhox13* were also expressed in a higher number of SP3 cells in *Topbp1*<sup>B5/B5</sup> (Supplemental Figures 25-26). In the case of *Scml2*, *Topbp1*<sup>B5/B5</sup> cells not only displayed an increased number of SP3 (pachytene) cells expressing it but also displayed an increase in expression levels in these cells compared to *Topbp1*<sup>+/+</sup> testes (Supplemental Figures 25-26). In summary, various Y and X genes that had previously been shown to be expressed in other MSCI-defective mutants were found de-repressed in *Topbp1*<sup>B5/B5</sup> spermatocytes.

Detailed analysis of the scRNA-seq data for the X-linked genes monitored during the early spermatocyte stages revealed important differences in the silencing dynamics of these X genes between *Topbp1*<sup>B5/B5</sup> and *Topbp1*<sup>+/+</sup> spermatocytes. 233 out of the roughly 700 genes present on the X chromosome had reads detected from pre-leptotene to spermatocyte 3 clusters for both

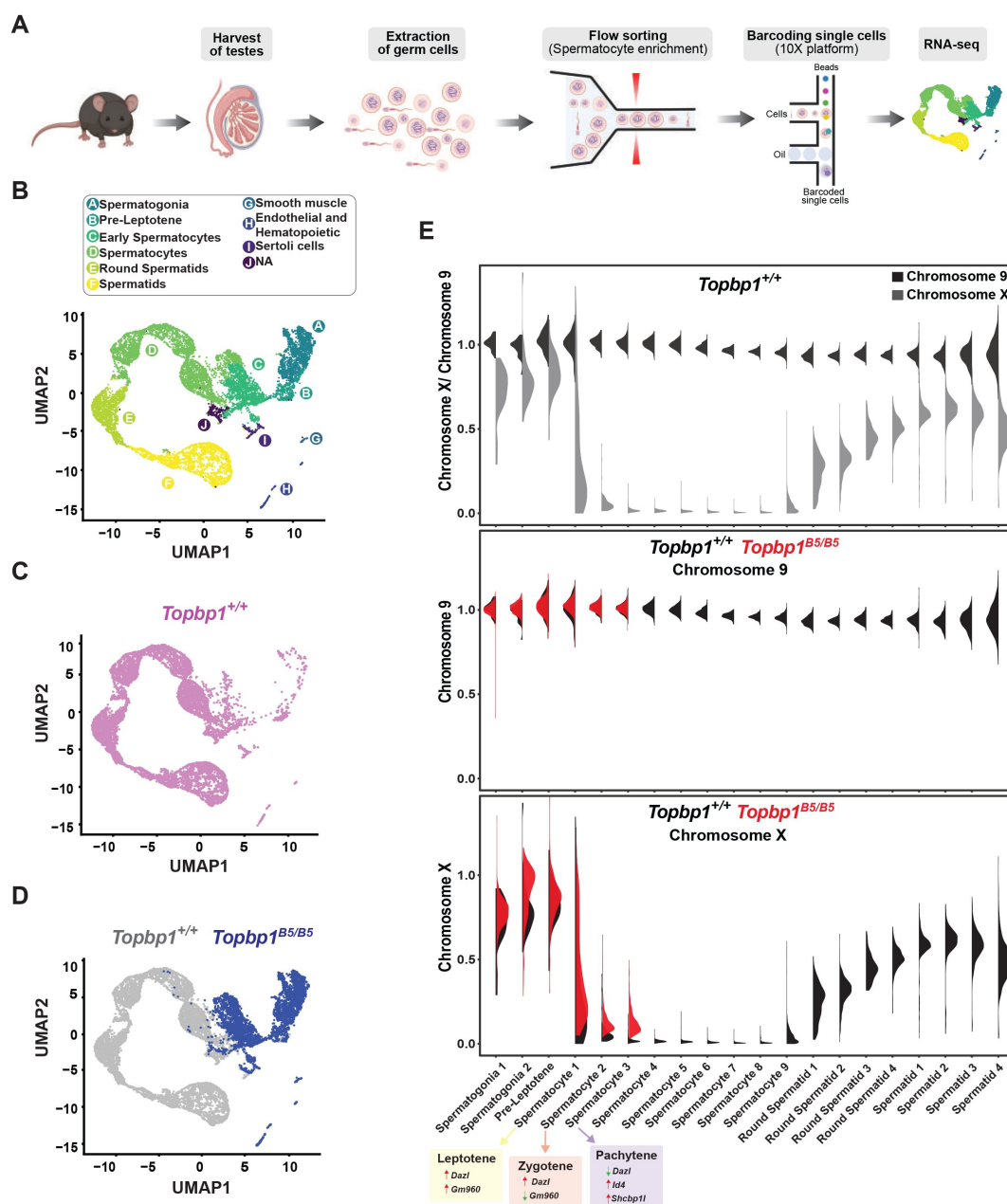


**Figure 6.**

### Single cell RNAseq reveals that *Topbp1*<sup>B5/B5</sup> spermatocytes initiate MSCI but fail to promote full silencing.

A) scRNAseq workflow for isolation and purification of single cells for RNA-seq. B) UMAP analysis of sub-clusters captured in the scRNAseq, representing all cells captured for both, *Topbp1*<sup>+/+</sup> and *Topbp1*<sup>B5/B5</sup>. C) UMAP analysis of sub-clusters captured in the scRNAseq of *Topbp1*<sup>+/+</sup>. D) UMAP analysis of sub-clusters captured in the scRNAseq of *Topbp1*<sup>+/+</sup> (gray) and *Topbp1*<sup>B5/B5</sup> (blue). E) Violin plots displaying the ratio of the average expression of X chromosome genes by the average expression of chromosome 9 genes at different stages of spermatogenesis for *Topbp1*<sup>+/+</sup> and *Topbp1*<sup>B5/B5</sup> cells. The level of X-genes expression in Spermatocyte 3 is significantly higher in *Topbp1*<sup>B5/B5</sup> cells when compared to *Topbp1*<sup>+/+</sup> cells, with a p-value of 1.5e-178 using a two-sided Wilcoxon rank sum test.

*Topbp1*<sup>+/+</sup> and *Topbp1*<sup>B5/B5</sup> cells, and therefore were used during the downstream analysis. As shown in **Figure 7A**, we clustered the X-linked genes into 3 distinct categories based on the change of RNA level between the stages: reduced, unaltered, or increased silencing (**Figures 7A–C**). SP1 (spermatocyte 1) was defined as leptotene using the gene marker *Gm960* (Chen et al., 2018) (Supplemental Figure 27), and SP2 (spermatocyte 2) as zygotene due to its profile of low expression of *Gm960* and high expression of *Dazl*. SP3 (spermatocyte 3) was defined as pachytene due to its lower expression of *Dazl* and increased expression of *Id4* and *Shcbp1l*. When comparing the distribution of genes in these clusters between *Topbp1*<sup>B5/B5</sup> and *Topbp1*<sup>+/+</sup> spermatocytes (RNA level normalized to pre-leptotene stage) (**Figure 7B**), we observed no major differences in the pre-leptotene to spermatocyte 1 (PL to SP1) and in the spermatocyte 1 to spermatocyte 2 (SP1 to SP2) transitions. In contrast, when comparing the spermatocyte 2 to spermatocyte 3 (SP2 to SP3) transition between *Topbp1*<sup>B5/B5</sup> and *Topbp1*<sup>+/+</sup> spermatocytes we noticed a major difference in the distribution of the clusters, with 74 genes in *Topbp1*<sup>B5/B5</sup> versus 4 in *Topbp1*<sup>+/+</sup> exhibiting reduced silencing (**Figure 7B**). Moreover, while 134 genes showed unaltered silencing, and only 24 increased silencing in *Topbp1*<sup>B5/B5</sup> spermatocytes during the SP2 to SP3 transition, 43 genes showed unaltered silencing and 185 increased silencing in *Topbp1*<sup>+/+</sup> (**Figure 7B**). *Xiap*, *Zc3h12b* and *Cetn2* are examples of X-linked genes displaying altered silencing behaviors in *Topbp1*<sup>B5/B5</sup> spermatocytes (**Figure 7C**). The difference of expression between *Topbp1*<sup>+/+</sup> and *Topbp1*<sup>B5/B5</sup> was markedly higher in the SP2 to SP3 transition compared to the other transitions (**Figure 7D–E**) and was used to further split genes into 3 categories based on the severity of the silencing defect in *Topbp1*<sup>B5/B5</sup>: no defect (13 genes), mild (45 genes) or strong defect (170 genes) (**Figure 7F**). Notably, the severity of the silencing defect of a gene had some correlation with its RNA level in the pre-leptotene stage, with highly expressed genes having a higher tendency to have a more severe silencing defect (**Figure 7G** and Supplemental Figure 28). Taken together, these data characterize the specific silencing defect in *Topbp1*<sup>B5/B5</sup> spermatocytes and point to a specific role for TOPBP1 in ensuring proper silencing dynamics after an initial wave of MSCI, likely through later waves of silencing reinforcement. Our data is consistent with the notion that silencing of the X and Y chromosomes is a dynamic process that needs active and continuous engagement by the ATR-TOPBP1 signaling axis. Since the majority of the mouse models of male infertility accumulate pleiotropic defects, with disrupted MSCI and absence of sex body, the *Topbp1*<sup>B5/B5</sup> mouse reported here provides a unique model of DDR impairment in which MSCI can be uncoupled from sex body formation (**Figure 8**).

## Discussion

In male meiosis I, DDR factors such as ATR, TOPBP1, BRCA1, and the 9-1-1 complex play crucial roles in DNA repair, chromosome synapsis, recombination, sex body formation, and silencing (Broering et al., 2014; ElInati et al., 2017; Pacheco et al., 2018; Pereira et al., 2022; Royo et al., 2013; Turner et al., 2004; Widger et al., 2018). Conditional depletion of these factors results in pleiotropic phenotypes from compound effects in multiple processes, with cells ultimately undergoing apoptotic-induced cell death during the pachytene checkpoint. Here, we report a mutant mouse model capable of deconvoluting TOPBP1's roles during meiosis I in males, separating its role in silencing from its roles in DNA repair, synapsis and checkpoint signaling (**Figure 8**). While *Topbp1*<sup>B5/B5</sup> spermatocytes initiate XY silencing with similar dynamics as observed in *Topbp1*<sup>+/+</sup> these cells fail to complete silencing at the final steps of MSCI. Of note, *Topbp1*<sup>B5/B5</sup> cells displayed slightly higher expression of X-linked genes than *Topbp1*<sup>+/+</sup> cells in the earlier spermatogenic stages (from spermatogonia 1 to spermatocyte 3). Furthermore, not all X-linked genes in *Topbp1*<sup>B5/B5</sup> spermatocytes were silenced; instead, some genes were only partially silenced while others exhibited increased expression after initial silencing. This is consistent with previous reports using mouse mutants with more severe MSCI defects, such as *Ago4*<sup>-/-</sup> and *Topbp1* CKO, in which not all X-linked genes exhibited altered levels of expression (ElInati et al., 2017; Modzelewski et al., 2012). Interestingly, a sex body is formed that is morphologically indistinguishable from the sex body in wild-type animals. Several heterochromatin markers, as



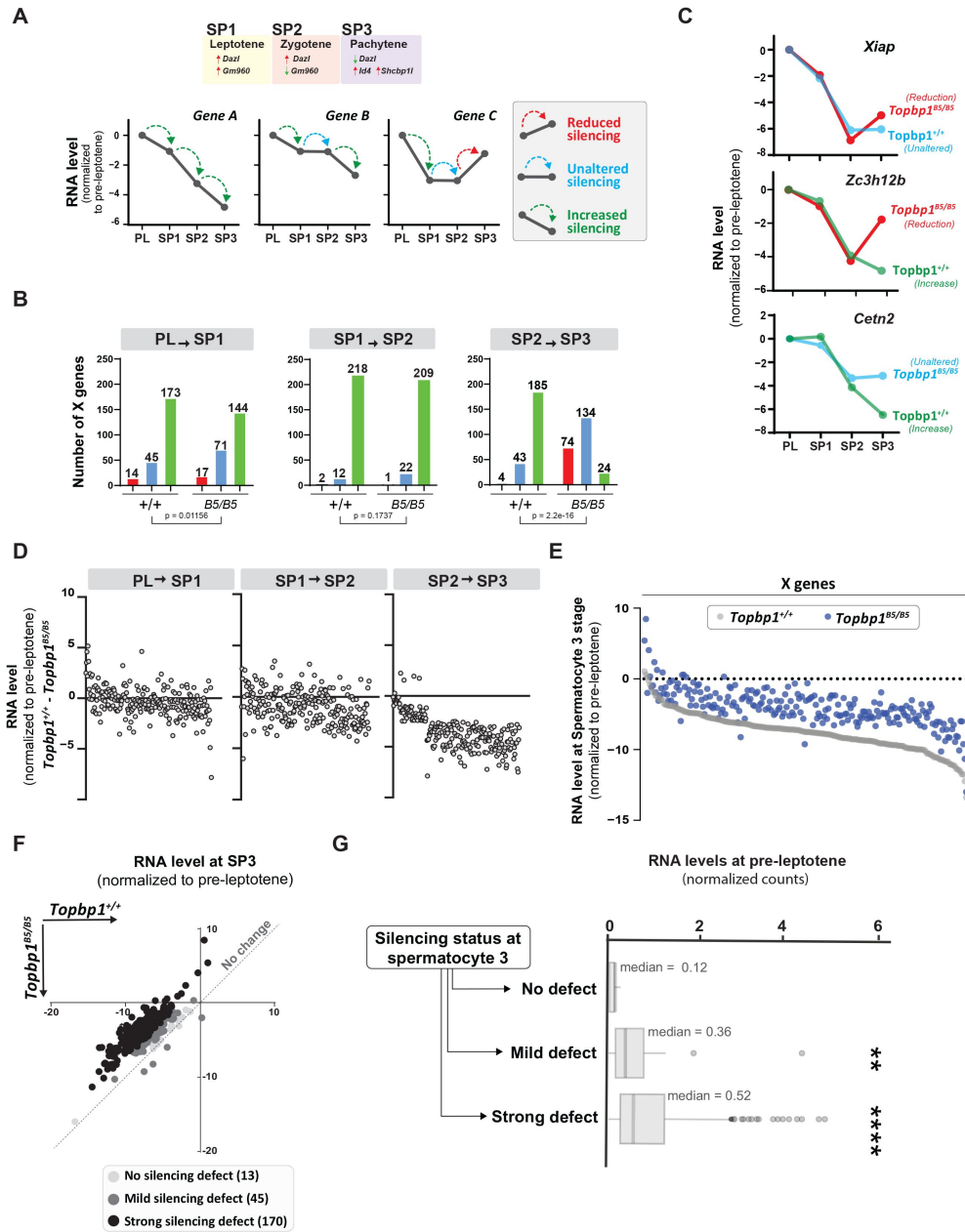


**Figure 7.**

### **Topbp1 regulates silencing dynamics of X genes at the Spermatocyte 3 stage.**

A) Illustration of the gene markers used to define spermatocyte 1 as leptotene, spermatocyte 2 as zygotene, and spermatocyte 3 as pachytene; hypothetical examples illustrating the categorization of transitions in silencing dynamics between the stages of pre-leptotene (PL), spermatocyte 1 (SP1), spermatocyte 2 (SP2), spermatocyte 3 (SP3). B) Number of genes in each of the categories described in A, during the different stage transitions and respective p-values above each graph (the p-values were calculated using the Fisher's exact test). C) Examples of genes with altered silencing dynamics in the *Topbp1*<sup>B5/B5</sup>, red = reduced silencing, blue = unaltered silencing and green = increased silencing D) Scatter plot showing the difference in RNA level between *Topbp1*<sup>+/-</sup> and *Topbp1*<sup>B5/B5</sup> for each of the indicated stage transitions. E) Scatter plot showing expression level of X-chromosome genes, normalized to pre-leptotene levels, in *Topbp1*<sup>+/-</sup> (gray) and *Topbp1*<sup>B5/B5</sup> (blue) at SP3. F) Graph plotting expression levels of X-chromosome genes, normalized to pre-leptotene levels, in *Topbp1*<sup>+/-</sup> (Y axis) and *Topbp1*<sup>B5/B5</sup> (X axis) and split in three categories based on the severity of silencing defect. G) Box plot showing PL expression levels of X-chromosome genes in each of the categories of silencing defect severity shown in F.

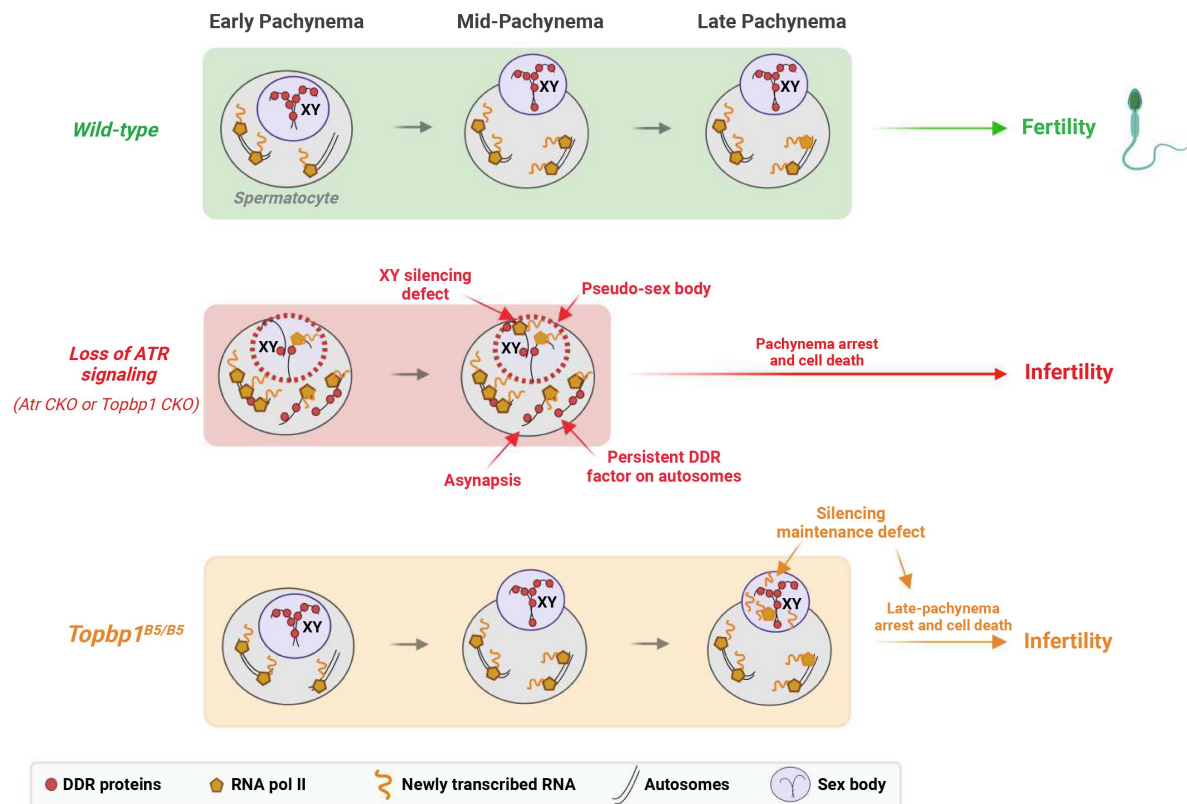


**Figure 8.**

### A new TOPBP1 mutant separates XY silencing from sex body formation.

Schematic of sub-stages of meiotic prophase I. In Wild-type mice, MSCI initiates following the accumulation of the DDR proteins at the XY chromosomes. During mid-pachytene, the XY body is fully formed, and transcription is restricted to the autosomes. In *Atr* or *Topbp1* CKOs, the sex body is not formed, and the DDR proteins are not sequestered to the XY. Asynapsis events and transcription of toxic genes at the sex chromosomes are observed, triggering mid-pachytene arrest. In *Topbp1*<sup>B5/B5</sup>, MSCI initiates, the sex body is normally formed with normal recruitment of DDR proteins to the X and Y chromosomes, yet cells fail in the reinforcement/maintenance of silencing. Cells progress through mid-pachytene but not into diplotene.

well as multiple canonical markers of sex body formation localize properly in the sex body of *Topbp1*<sup>B5/B5</sup> mice. Overall, these findings suggest a non-canonical role for the ATR-TOPBP1 signaling axis in ensuring proper XY silencing dynamics during pachynema. This is the first DDR mutant that separates XY silencing from sex body formation, and that separates TOPBP1's role in spermatogenesis from its roles in organismal viability.

The *B5* allele reported here, which carries eight lysine to glutamic/aspartic acid substitutions in BRCT domain 5, is the first mutation shown to impair the meiotic silencing function of TOPBP1 in spermatocytes without severely disturbing TOPBP1's role in synapsis and sex body formation. Consistent with this being a separation of function mutant, *Topbp1*<sup>B5/B5</sup> males are viable and grossly normal, while completely sterile, whereas *Topbp1* null, or AAD mutated, mice are embryonic lethal (Jeon et al., 2011 [DOI](#); Zhou et al., 2013 [DOI](#)). Moreover, depletion of TOPBP1 in mammalian cell lines triggers a robust G2/M arrest followed by cell senescence and loss of viability (Jeon et al., 2011 [DOI](#)). *Topbp1*<sup>B5/B5</sup> MEFs do not display issues with cell proliferation or DDR defects. Based on these observations, and the finding of a silencing defect in *Topbp1*<sup>B5/B5</sup> spermatocytes, it is likely that the role of TOPBP1 in silencing documented here could be specifically relevant in the context of male meiosis. It is important to note that other mutants previously reported to have XY silencing defects during meiotic prophase I, such as *Ago4* null and *Dicer* CKO, do not result in complete loss of sperm production, but a sub-fertility phenotype (Greenlee et al., 2012 [DOI](#); Modzelewski et al., 2012 [DOI](#)). Therefore, we speculate that the specific type of silencing defect in *Topbp1*<sup>B5/B5</sup> spermatocytes is particularly toxic, similar to other mutations in the DDR pathway that result in MSCI defects, which would explain the highly penetrant defect in sperm production.

The model that distinct TOPBP1 interactions mediate distinct ATR signaling pathways offers a potential explanation for why *Topbp1*<sup>B5/B5</sup> have specific defects in silencing without noted effects in other key processes regulated by ATR, such as synapsis. In addition to binding and activating ATR through its AAD domain (Mordes et al., 2008 [DOI](#); Pereira et al., 2020 [DOI](#)), TOPBP1 can bind to several proteins through its BRCT domains (Yamane et al., 2002 [DOI](#)) and act as a scaffolding protein to bring substrates in close proximity to ATR, thus facilitating the propagation of specific ATR signaling pathways. Experiments using ectopic expression of Flag-tagged TOPBP1 in HEK293T cells revealed that the set of mutations in *B5* disrupt the ability of TOPBP1 to interact with 53BP1 and BLM, as expected from previous reports (Bigot et al., 2019 [DOI](#); Blackford et al., 2015 [DOI](#); Cescutti et al., 2010 [DOI](#); Liu et al., 2017 [DOI](#); Wang et al., 2013 [DOI](#)). However, it is unclear if the same interactions are also disrupted in spermatocytes, or whether additional TOPBP1 interactions mediated by its BRCT5 specifically during meiotic prophase I are also disrupted. Apart from disrupting protein interactions, it is also possible that the observed changes in TOPBP1 protein stability in the *Topbp1* *B5* mutant can contribute to impairing its roles in silencing. Such change in protein stability is consistent with a previous report showing that the TOPBP1-BLM interaction contributes to protein stabilization (Balbo Pogliano et al., 2022 [DOI](#); Wang et al., 2013 [DOI](#)). Further work will be necessary to determine if the phenotypes observed in *Topbp1*<sup>B5/B5</sup> spermatocytes are caused specifically by disruption of specific protein interactions, or by a combination of disrupted interactions and reduced protein abundance. It is worth mentioning that the *Topbp1*<sup>B5/B5</sup> phenotype is distinct from the *Topbp1* CKO despite the reduction in protein abundance.

Our finding that SETX localization to chromatin loops of the XY is impacted in *Topbp1*<sup>B5/B5</sup> pachytene spermatocytes, together with our previous report that SETX undergoes ATR-dependent phospho-regulation in spermatocytes (Sims et al., 2022 [DOI](#)), suggest that an ATR-TOPBP1-SETX signaling axis is important for the silencing reinforcement in late MSCI. Genetic data support that impairment of this specific signaling axis would impact silencing without impacting synapsis. For example, *Topbp1* CKO, *Rad1* CKO, and *Atr* CKO spermatocytes display strong synapsis defect and defective entry in pachynema (ElInati et al., 2017 [DOI](#); Widger et al., 2018 [DOI](#)), whereas *Setx* null spermatocytes complete autosomal synapsis, while still displaying MSCI defects. On the other hand, it is likely that ATR signaling is controlling a specific aspect of SETX function since

*Topbp1*<sup>B5/B5</sup> spermatocytes do not share all defects observed in *Setx* null spermatocytes, as noted by the localization of  $\gamma$ H2AX, sumoylation events, ubH2A and ATR at chromatin loops, which are defective in *Setx* null spermatocytes but normal in *Topbp1*<sup>B5/B5</sup> spermatocytes. Moreover, *Topbp1*<sup>B5/B5</sup> pachytene spermatocytes, but not *Setx* null spermatocytes, are able to reach the stage of crossover designation with MLH1 positive cells. Taken together, these observations suggest that *Topbp1*<sup>B5/B5</sup> pachytene spermatocytes progress further in pachynema when compared to *Setx* null spermatocytes and are consistent with a model in which a ATR-TOPBP1 control only specific(s) mode of SETX regulation (Pereira et al., 2022 [↗](#); Sims et al., 2022 [↗](#)).

The model involving SETX as a potential factor by which ATR controls silencing late in MSCI opens exciting directions to explore the interface of ATR-TOPBP1 with RNA processing. Given the established role for SETX in the resolution of R-loops (Bennett and La Spada, 2018 [↗](#)), it is tempting to speculate that silencing defects in *Topbp1*<sup>B5/B5</sup> mutant may be related to aberrant accumulation of RNA-DNA hybrids that may affect removal of nascent mRNAs that is necessary for imposing silencing. This hypothesis assumes that the silencing of X and Y genes is a dynamic process involving ongoing mechanisms of exclusion of RNA polymerase II and nascent RNA, as proposed recently (Abe et al., 2022 [↗](#); Sims et al., 2022 [↗](#)). Moreover, the model predicts that SETX function is specifically affected in the sex body, which is consistent with the observed defect in SETX localization. In support of this model, R-loops affect chromatin architecture at promoters and interfere with the recruitment of transcription factors and chromatin remodelers, as observed in regions harboring CpG islands where R-loops prevent the action of DNA methyltransferases, thus preventing silencing (Santos-Pereira and Aguilera, 2015 [↗](#)). Notably, highly transcribed genes, which tend to accumulate more R-loops (Marnef and Legube, 2020 [↗](#)), displayed increased silencing defects in the *Topbp1*<sup>B5/B5</sup> mutant.

While we have provided strong evidence to suggest a defect in later stages of MSCI as the cause of the cell death observed in *Topbp1*<sup>B5/B5</sup> spermatocytes, we cannot exclude the potential contribution of other defects, beyond silencing, to the loss of diplotene cells. The increased number of MLH1 foci suggested an altered recombination pattern, possibly impairing the ratios of class I and class II crossovers. The BRCT 5 domain of TOPBP1 interacts with the BLM helicase (Balbo Pogliano et al., 2022 [↗](#); Blackford et al., 2015 [↗](#)), which has been found to play a role in meiotic recombination in yeast and mice (Holloway et al., 2010 [↗](#); Rockmill et al., 2003 [↗](#)). *Blm* CKO mice display severe defects in prophase I progression in spermatocytes, including, incorrect pairing and synapsis of homologs, and defective processing of recombination intermediates, leading to increased chiasmata (Holloway et al., 2010 [↗](#)). These observations raise the possibility that impaired meiotic progression and cell death in *Topbp1*<sup>B5/B5</sup> spermatocytes is a combination of defects in MSCI and recombination. *Topbp1*<sup>B5/B5</sup> spermatocytes do not progress beyond pachytene hence we were not able to visualize chiasmata and directly infer whether or not *Topbp1*<sup>B5/B5</sup> is defective in crossing over. Of note, MLH1 and MLH3 are known to form a heterodimer in the context of meiotic recombination (Lipkin et al., 2000 [↗](#); Svetlanov et al., 2008 [↗](#)). While our data show increased MLH1 foci counts in *Topbp1*<sup>B5/B5</sup>, MLH3 foci counts were not different from *Topbp1*<sup>+/+</sup>, thus, we cannot exclude the possibility that the imbalance between MLH1 and MLH3 might affect the loss of diplotene cells in *Topbp1*<sup>B5/B5</sup> through processes not related to crossing over. Importantly, while MLH3 works exclusively as a heterodimer with MLH1, MLH1 can function in a heterodimeric complex with other MutL homologs (Nakagawa et al., 1999 [↗](#)).

Our findings showing that TOPBP1 plays a specific role in silencing reinforcement after the first wave of MSCI are consistent with the recently proposed notion that the establishment and maintenance of MSCI is a dynamic process (Abe et al., 2022 [↗](#); Sims et al., 2022 [↗](#)). Also consistent with this notion is our recent finding showing that ATR signaling is itself also highly dynamic and constantly being cycled (Sims et al., 2022 [↗](#)). For example, using mice treated with the ATR inhibitor (ATRi) AZ20 for four hours, we found that such a short treatment is already sufficient to cause a complete loss of  $\gamma$ H2AX, pMDC1 and SETX localization from the XY chromosomes (Abe et al., 2022 [↗](#); Sims et al., 2022 [↗](#)). Furthermore, germ cells subjected to ATRi for 24 hours showed

complete recovery of  $\gamma$ H2AX only three hours after release from ATRi treatment (Abe et al., 2022 [DOI](#)). We propose that TOPBP1 acts on this phospho-cycle to ensure proper silencing reinforcement and maintenance, potentially by counteracting the engagement of anti-silencing factors that dynamically enter the sex body and need to be actively antagonized at the XY. Future work involving the characterization of possible unknown interactors of the BRCT domain 5 of TOPBP1, as well as functional dissection of ATR targets in MSCI, is essential to understand how TOPBP1 modulates the silencing machinery and shapes silencing dynamics. Interestingly, while we propose that the lack of silencing maintenance is the major defect causing the pachytene cell death in *Topbp1*<sup>B5/B5</sup> spermatocytes, we cannot exclude the possibility that the expression of XY-linked genes could represent a regulated response to meiotic defects more than a mere consequence of a defective MSCI. If this latter hypothesis is true, the cell death caused by defects in the XY chromosomes would be independent of MSCI. Notably, this hypothesis could not have been conceptualized prior to this work given that the majority of prophase I mutants characterized to this date are unable to reach the stage where MSCI is properly established. Thus, the *Topbp1*<sup>B5/B5</sup> is a unique model allowing future studies that may uncouple MSCI from XY-triggered cell death during pachynema.

In summary, our study presents a unique model for investigating the role of DDR factors in XY silencing. By allowing the uncoupling of MSCI progression from sex body formation, the *Topbp1*<sup>B5/B5</sup> mutant enables the study of MSCI dynamics during key stages late in pachynema. Notably, the inability of *Topbp1*<sup>B5/B5</sup> to sustain or reinforce silencing opens the possibility of uncovering new insights into the MSCI-dependent pachytene checkpoint.

## Materials and methods

### Key resource table



Reagent type	Designation	Source or Reference	Identifiers	Additional information
Primer	p3xflag-TOPBP1-Flag-N-terminal-F	IDT	PCR primer	attcatcgatagatctgata ATGTCCAGAAAT GACAAAGA
Primer	p3xflag-TOPBP1-Flag-N-terminal-R	IDT	PCR primer	tagagtcgactggtaccgat ttagTGTACTIONCTAG GTCGTT
Primer	hTopbp1_K1317A_R	IDT	Site-directed mutagenesis	tgccactgaggctaatac gcctcggttcgaagtggatg t
Primer	hTopbp1_K1317A_F	IDT	Site-directed mutagenesis	acatccacttcgaacgag gcgtatttagcctcagtggc a
Primer	hTopbp1_K155A_F	IDT	Site-directed mutagenesis	caggtttgagcaactaaat atgcttgctaccaactctc ctgca
Primer	hTopbp1_K155A_R	IDT	Site-directed mutagenesis	tgcaggagaagtggtagc aaagcatatttagtgctgca aacctg
Primer	hTopbp1_K250A_R	IDT	Site-directed mutagenesis	tctcttgccacactcatacg cctgaccttttggtcttgc
Primer	hTopbp1_K250A_F	IDT	Site-directed mutagenesis	gcaagaacaaaagggtca ggcgtatgagtggtccaag aga
Primer	musTopbp1_BRCT5-Fwd genotyping	IDT	PCR primer	tgcatttcattaaccaacct c
Primer	musTopbp1_BRCT5 Rev genotyping	IDT	PCR primer	ggtagagttcaaatgtgtgt catg
Antibody	phospho H2A.X (Ser139)	Millipore	Cat# 05-636;RRID:AB_309864	IF (meiotic spreads) 1:50000 IF 1:2000

Antibody	SCP3 antibody	Abcam	Cat# ab97672;RRID: AB_10678841	IF (meiotic spreads) 1:1000
Antibody	SYCP3	(Lenzi et al., 2005)	Custom	IF (meiotic spreads) 1:10000
Antibody	SCP1	Abcam	ab15090	IF (meiotic spreads) 1:1000
Antibody	Rad51	Millipore	PC130	IF (meiotic spreads) 1:1000
Antibody	ATR	Cell signaling	2790	IF (meiotic spreads) 1:1000
Antibody	TOPBP1	(Danielsen et al., 2009)	Custom	IF (meiotic spreads) 1: 500 Western blot 1:1000
Antibody	phospho-Chk1 (ser317)	Cell Signaling	12302	IF (meiotic spreads) 1: 100 Western blot 1:1000
Antibody	H1T	A gift from Dr. Mary Ann Handel (Inselman et al., 2003)	Custom	IF (meiotic spreads) 1: 500
Antibody	HORMAD2	(Wojtasz et al., 2012)	Custom	IF (meiotic spreads) 1: 500
Antibody	HORMAD1	(Wojtasz et al., 2012)	Custom	IF (meiotic spreads) 1: 500
Antibody	phospho HORMAD2 (S271)	(Wojtasz et al., 2009)	Custom	IF (meiotic spreads) 1: 500
Antibody	GAPDH	Thermo Fisher Scientific	AM4300	Western blot 1:5000
Antibody	$\beta$ -Actin	Cell Signaling	4967	Western blot 1:5000
Antibody	phospho MDC1 (T4)	Abcam	Ab35967	IF (meiotic spreads) 1: 500

Antibody	SETX	Abcam	Ab220827	IF (meiotic spreads) 1: 100
Antibody	SETX	Novus Biologicals	NBP1-94712SS	Western blot 1:1000
Antibody	MLH1	BD Biosciences	550838	IF (meiotic spreads) 1: 200
Antibody	MLH3	A gift from Dr. Paula Cohen (Holloway et al., 2014)	Custom	IF (meiotic spreads) 1: 200
Antibody	CHK1	Santa Cruz	sc-8408	Western blot 1:1000
Antibody	CHK2	Millipore	05-649 (clone7)	Western blot 1:1000
Antibody	phospho CHK1 (S345)	Cell Signaling	2341	IF (meiotic spreads) 1: 200 Western blot 1:1000
Antibody	phospho RPA (S4/S8)	Bethyl	A300-245A,	Western blot 1:1000
Antibody	RPA (made against full length RPA2 expressed and purified in <i>E. Coli</i> and injected to rabbit)	N/A	Custom	Western blot 1:1000
Antibody	KAP1	Bethyl	a700-014-T	Western blot 1:1000
Antibody	phospho KAP1 (S824)	Bethyl	A300-767A-T	Western blot 1:1000
Antibody	53BP1	Cell signaling	4937	Western blot 1:1000
Antibody	53BP1	Novus Biologicals	NB100-304	IF (meiotic spreads) 1: 200
Antibody	BLM	Abcam	ab2179	Western blot 1:500
Antibody	Rad9	Bethyl	A300-890A-T	Western blot 1:1000
Antibody	BRCA1	(Kakarougk as et al.,	Custom	IF (meiotic spreads) 1: 200

		2013)		
Antibody	BRCA1	Proteintech	22362-1-AP	Western blot 1:1000
Antibody	MDC1	(Modzelews ki et al., 2015)	Custom	IF (meiotic spreads) 1: 200 IF 1: 200
Antibody	RNA pol 2	Millipore	05-623	IF (meiotic spreads) 1: 2000
Antibody	phospho RNA pol 2 (Ser2)	Millipore	04-1571	IF (meiotic spreads) 1: 400
Antibody	phospho RNA pol 2 (Ser5)	Millipore	04-1572	IF (meiotic spreads) 1: 400
Antibody	H3K9ac	Abclonal	A7255	IF (meiotic spreads) 1: 200
Antibody	H3K9me3	Active Motif	39766	IF (meiotic spreads) 1: 200
Antibody	H3K4me1	Abclonal	A2355	IF (meiotic spreads) 1: 200
Antibody	CHD4	Abclonal	A10557	IF (meiotic spreads) 1: 200
Antibody	Sumo_2/3	Proteintech	G67154-1-1g	IF (meiotic spreads) 1: 200
Antibody	USP7	Proteintech	66514-1-Ig	IF (meiotic spreads) 1: 200
Antibody	H3K27ac	Active Motif	39134	IF (meiotic spreads) 1: 200
Antibody	H3K36ac	Active Motif	61102	IF (meiotic spreads) 1: 200
Antibody	H3K4me3	Active Motif	39160	IF (meiotic spreads) 1: 200
Antibody	H4K16ac	Abclonal	A5280	IF (meiotic spreads) 1: 200
Antibody	H4c	Millipore	06-598	IF (meiotic spreads)

				1: 200
Antibody	H2AK199ub	Abcam	Ab193203	IF (meiotic spreads) 1: 200
Antibody	Goat anti-rabbit IgG (H + L) highly cross-adsorbed secondary antibody, Alexa Fluor 488	Thermo Fisher Scientific	A-11034	IF (meiotic spreads) 1: 1000
Antibody	Goat anti-mouse IgG (H + L) antibody, Alexa Fluor 488 conjugated	Thermo Fisher Scientific	A-11017	IF (meiotic spreads) 1: 1000
Antibody	Goat anti-rabbit IgG (H + L) antibody, Alexa Fluor 594 conjugated	Thermo Fisher Scientific	A-11012	IF (meiotic spreads) 1: 1000
Antibody	Goat anti-mouse IgG (H + L) highly cross-adsorbed secondary antibody, Alexa Fluor Plus 594	Thermo Fisher Scientific	A32742	IF (meiotic spreads) 1: 1000
Antibody	Goat anti-guinea pig IgG (H + L) highly cross-adsorbed secondary antibody, Alexa Fluor 647	Thermo Fisher Scientific	A-21450	IF (meiotic spreads) 1: 1000
Commercial assay or kit	ApopTag Plus Peroxidase In Situ Apoptosis Kit	Millipore	S7101	N/A
Software, algorithm	GraphPad Prism 9	GraphPad Prism	RRID:SCR_002798	N/A
Software	Cellranger v7.0.0	10X Genomics	<a href="https://support.10xgenomics.com/single-cell-gene-expression/software/download">https://support.10xgenomics.com/single-cell-gene-expression/software/download</a>	N/A



			s/3.1	
Software	R v4.2.1	R Foundation	RRID:SCR_001905	N/A
Software	Seurat v4.3.0	(Hao et al., 2021)	RRID:SCR_007322	N/A
Software	sva v3.44.0	(Leek et al., n.d.)	RRID:SCR_012836	N/A
Software	SingleR v1.10.0	(Aran et al., 2019)	RRID:SCR_023120	N/A
Software	Reshape2 v1.4.4	(Wickham, 2007)	RRID:SCR_022679	N/A
Software	biomaRt v2.52.0	(Durinck et al., 2009)	RRID:SCR_019214	N/A
Software	ggpubr v0.5.0	(Kassambara, 2019)	RRID:SCR_021139	N/A
Software	Tidyverse v1.3.2	(Wickham et al., 2019)	RRID:SCR_019186	N/A
Software	ggnewscale v0.4.8	Campitelli	<a href="https://eliocamp.github.io/ggnewscale/index.html">https://eliocamp.github.io/ggnewscale/index.html</a>	N/A

Software	Harmony v0.1.1	(Korsunsky et al., 2019)	RRID:SCR_022206	N/A
Software	Org.Mm.eg.db v3.15.0	(Carlson et al., n.d.)	RRID:SCR_023488	N/A
Software	Corrplot v0.92	(Wei and Simko, 2017)	RRID:SCR_023081	N/A
Software	SeuratWrappers v0.3.1	Satija Lab	RRID:SCR_022555	N/A
Software	gghalves v0.1.4	Tiedemann	<a href="https://github.com/erocoar/gghalves">https://github.com/erocoar/gghalves</a>	N/A

## Resource availability

### Lead contact

Further information and requests for resources and data should be directed to and will be fulfilled by the lead contact, Marcus Smolka (email: [mbs266@cornell.edu](mailto:mbs266@cornell.edu)).

### Materials availability

This study generated a unique antibody, RPA.

## Mice, genotyping and treatment of mice with IR

All mice used in this work were handled following federal and institutional guidelines under a protocol approved by the Institutional Animal Care and Use Committee (IACUC) at Cornell University. CRISPR/Cas9 editing was used to engender the *Topbp1B5* allele and performed by the Cornell Mouse Modification core facility. To this end, the online tools CRISPR gold and ChopChop were used to generate high quality (guide score >9) CRISPR guide RNAs targeting the intronic sequences neighboring the genomic sequence of *Mus musculus topbp1* exon 13. The CRISPR crRNAs (purchased from IDT) harboring the sequences ccaactcaggtcgccgctcttg and cctcgattagtctcaaggcgag (PAM sites are underlined), both targeting the reverse strand, the repair template (below), and CAS9 RNA were injected on embryos from super ovulated, plugged C57BL/6J female mice crossed to C57BL/6J stud males. 2-cell stage embryos were then implanted on pseudo pregnant females and pups were genotyped after one week old.

Repair template:

```
acagcagggtcttctgtgtaaccctctctccgtagaccagtttggccttgatcgaaactcaggtcgccgctcttgctcttagagtctctgggat
taaaggcgtgcactgccaccaccagagatgtttctctgacattaacatgctatttttttaaatgagctaattgtgttcatttgctttattt
ccatgtaaaatttagTGTTCAAGAATTCTTTGTTGACGAAGCCAATGCAGAGGAAGGCATGCT
```

CGCCAGCACACATCTTATAGTGGAGGAACCGACTGGTTCCGAATACGAAGCTGCAG  
 AGGAATGGAGTTTGCCGGCAGTTAACATTTTCATGGCTCTTAGAACTGCGGAAATCG  
 GGGAGGAAGCAGATGAAAACCATTTTCTGGTTGACAACGCACCTAAACAAGgttagaagt  
 cctgttttttttatgtattttacaacttgatggtttctgaaataggatgttcagttactgctttaaaacattgtatgaccctaacctcagtcagtg  
 gtgcttacttcagaacctgagtgaaacacggaagcagatcaatgaagaagcgcacagggtaacggctgattagctcctcaaggcga  
 gtgacgagaaggtgacccccga atggctgttagaagcagttttata (purchased from IDT as a G-block)

Intronic sequence is shown in lower case, exon 13 sequence is shown in capital letters; underline represents the mutated residues, pink represents the mutated PAM residues, in orange is shown the guide RNA sequences and in red, the targeted amino acid sequences. Of note, although this repair template encodes for 11 amino acid changes, only 8 were successfully inserted into the mouse topbp1 exon 13 locus. For mice genotyping, the following primers were used 5'-tgcatctccattaaccaacctc-3' and 5'-ggtagagttcaaatgtgtcatg-3' (also shown at key resources table). For irradiation, *Topbp1*<sup>+/+</sup> and *Topbp1*<sup>B5/B5</sup> mice were placed in a 137 Cesium-sealed source irradiator (J.L. Shepherd and Associates) with a rotating turntable and irradiated with 7 Gy IR.

## MEFs and cell survival assays

MEFs were prepared from E13.5 mouse embryos as previously described (Balmus et al., 2012). Briefly, embryos were dissected and mechanically disrupted using pipette aspiration until homogenous. Cells were allowed to settle, and the supernatant was transferred into Dulbecco's modified medium supplemented with 10% fetal bovine serum, 1% penicillin/streptomycin and 1% nonessential amino acids. Following four days of growth, cells were then immortalized by transduction with a large-T antigen lentivirus. Subsequently, cells were selected with 10 µg/mL puromycin.

For colony survival assays, 500 cells were seeded per 10 cm dish, allowed to adhere for 24h and treated with Phleomycin or Hydroxyurea for 24h (drug concentrations are displayed on **figure 2A** - D and Supplemental Figure 2). In the following day, cells were released and let to form colonies for 10-15 days. Cells were then washed once with PBS, fixed in 100% methanol for 1h, stained with 0.1% crystal violet (MP Biomedicals, 152511) solution overnight, and then washed with distilled water before imaging and counting.

For accessing DDR and checkpoint responses via western blot, 2 x 10<sup>6</sup> cells were seeded on a 60 cm dish, allowed to adhere for 24h, and treated with Phleomycin or Hydroxyurea for 3h (drug concentrations are displayed on **Figure 2**).

## Cell culture

HEK-293T cells were cultured in Dulbecco's modified medium supplemented with 10% fetal calf serum, 1% penicillin/streptomycin and 1% nonessential amino acids. Immortalized MEFs were cultured in Dulbecco's modified medium supplemented with 10% fetal calf serum, 1% penicillin/streptomycin, 1% nonessential amino acids, and 1% glutamine supplementation. All cells were kept at 37°C and 5% CO<sub>2</sub>. All the cell lines were regularly tested for mycoplasma contamination with the Universal Mycoplasma Detection Kit (ATCC). HEK-293T cells were transfected using homemade polyethylenimine (Polysciences, Inc.). 36h after transfection, cells were treated with 1mM HU (Hydroxyurea) and then harvested for immunoprecipitation experiments.

## Plasmids

The full-length TOPBP1 CDS was cloned on a p3xflag vector (Milipore/Sigma E7658) using Gibson assembly (NEB) following the manufacturer's instructions. The p3xflag-TOPBP1 was used as a template to generate p3xflag-TOPBP-K155A, p3xflag-TOPBP-K250A, p3xflag-TOPBP-K704A, p3xflag-TOPBP-K1317A through site-directed mutagenesis using prime STAR master mix (Takara) and

Gibson assembly to generate p3xflag-TOPBP-KE, using the following G-block (IDT) containing the 8 charge-reversal point mutations at the BRCT 5 domain of TOPBP1:

```
AACGAATCCAATGCAGAAGAAGGCATGTTTGCCAGTACTCATCTTATACTGGAAGA
ACGTGGTGGCTCTGAATATGAAGCTGCAAAGAAGTGAATTACCTGCCGTACTAT
AGCTTGGCTGTTGGAGACTGCTAGAACGGGAGAAGA.
```

All primers used for the cloning are shown in the key resources table.

## Immunoblotting

Cells were harvested and lysed in modified RIPA buffer (50 mM Tris-HCl, pH7.5, 150 mM NaCl, 1% Tergitol, 0.25% sodium deoxycholate, 5 mM ethylenediaminetetraacetic acid (EDTA)) supplemented with complete EDTA-free protease inhibitor cocktail (Roche), 1 mM phenylmethylsulfonyl fluoride (PMSF) and 5 mM NaF. Whole cell lysates, after sonication, were cleared by 15 min centrifugation at 17,000 xg at 4°C. Twenty micrograms of protein extract were mixed with 3X sodium dodecyl sulfate sample buffer and resolved by SDS-PAGE. Gels were transferred on polyvinylidene difluoride membranes and immunoblotted using standard procedures. Western blot signal was acquired with a Chemidoc Imaging System (BioRad). Antibody information is provided in the key resources table.

## Immunofluorescence

MEFs were grown on coverslips and then submitted to IR, 5 gy and allowed to recover for 1.5h at 37°C and 5% CO<sub>2</sub>. Cells were then fixed using 3.7% formaldehyde in phosphate-buffered saline (PBS) for 10 min at room temperature (RT). Fixed cells were then washed 3x with PBS, permeabilized for 5 min with 0.2% Triton X-100/PBS at RT and blocked in 10% bovine serum albumin/PBS for 20 min at RT. Coverslips were incubated first with primary antibodies for 2h at RT, followed by three washes with PBS, and then for 1 hour with relative secondary antibodies. After incubation with secondary antibodies, coverslips were washed three times with PBS and then mounted on glass microscope slides using DAPI-Vectashield mounting medium (Vector Laboratories). Slides were imaged on a Leica DMI8 Microscope with a Leica DFC9000 GTC camera using the LAS X (Leica Application Suite X) software with a 100x objective. For micronuclei scoring, ~150–200 cells/replicate were counted. The two-tailed Student's t-test was used for statistical analysis. Antibody information is provided in the key resources table.

## Meiotic Spreads

Meiotic surface spreads were performed from 8- to 12-week-old mice as described by Kolas et al., (Kolas et al., 2005 [DOI](#)). Briefly, decapsulated testis from mice were incubated on ice in a hypotonic extraction buffer for 45 min. Tubules were then minced into single- cell suspension in 100 mM sucrose, and cells were spread on slides coated with 1% PFA with 0.15% TritonX- 100 and incubated in a humidifying chamber for 4h. For immunostaining, slides were blocked using 10% goat serum and 3% BSA, followed by incubation overnight with primary antibody (listed in the key resources table) at 4°C in a humidifying chamber. Secondary antibodies were incubated at 37°C for 2h in the dark, and slides were then cover-slipped using antifade mounting medium (2.3% DABCO, 20 mM Tris pH 8.0, 8 µg DAPI in 90% glycerol). Slides were imaged on a Leica DMI8 Microscope with a Leica DFC9000 GTC camera using the LAS X (Leica Application Suite X) software. For every condition, a minimum of 50 images from at least two independent mice were acquired. To quantify fluorescence intensity, the LAS X software quantification tool was used as previously described (Sims et al., 2022 [DOI](#)). Antibody information is provided in the key resources table. p-Values were calculated in Prism - GraphPad using a linear mixed effect model (Nested t test) that takes into account the variability in cells within each mouse when comparing mice between groups (*Topbp1*<sup>+/+</sup> vs *Topbp1*<sup>B5/B5</sup>).

### 3D-Structured Illumination super resolution Microscope (3D-SIM)

Higher resolution images were acquired using an ELYRA 3D-Structured Illumination Super Resolution Microscopy (3D-SIM) from Carl Zeiss with ZEN Black software (Carl Zeiss AG, Oberkochen, Germany). Images are shown as maximum intensity projections of z stack images. To reconstruct high-resolution images, raw images were computationally processed by ZEN Black. The brightness and contrast of images were adjusted using ImageJ (National Institutes of Health, USA). Antibody information is provided in the key resources table.

### Fertility assays

For fertility testing, 8 weeks old *Topbp1*<sup>B5/B5</sup> females and C57BL/6 males or C57BL/6 females and *Topbp1*<sup>B5/B5</sup> males were singly housed, where pregnancies were monitored for a period of one month. Viable pups were counted on the first day of life. For *Topbp1*<sup>B5/B5</sup> males, breeding cages remained active for a period of six months and at no time pregnant females nor birth of pups were detected. No noticeable defects were found on fertility of *Topbp1*<sup>B5/+</sup>, males or females (data not shown).

### Tunel

TUNEL assay was conducted using the Apoptag kit (EMD Millipore) following the manufacturer's instructions. The data were quantified in Image Scope by counting the number of positive cells per tubule for 100 tubules of each genotype, 3 mice each. Statistical differences between *Topbp1*<sup>+/+</sup> and *Topbp1*<sup>B5/B5</sup> were analyzed using Welch's unpaired t- test in GraphPad.

### Hematoxylin and eosin staining

Adult testes - from 12 weeks old mice - were dissected and incubated in Bouin's fixative overnight, washed during 30 min each in 30%, then 50% and then 70% ethanol. The 70% ethanol wash was repeated 3 times more. Testes were then embedded in paraffin. 5 µm sections were mounted on slides. After rehydration in Safe Clear Xylene Substitute followed by decreasing amounts of ethanol, slides were stained with hematoxylin followed by eosin. The slides were then gradually dehydrated by incubation in increasing concentrations of ethanol before mounting using toluene mounting medium.

### Epididymal sperm counts

Caudal and epididymides from 8- to 12-week-old mice were minced with fine forceps at 37°C in a Petri dish containing Dulbecco's modified medium supplemented with 10% fetal calf serum, 1% penicillin/streptomycin, 4% BSA, and 1% nonessential amino acids. Samples were then incubated at 37°C for 30 min allowing sperm to swim out into the media, then fixed in 10% neutral-buffered formalin (1:25 dilution). Sperm cells were counted using a hemocytometer and analyzed statistically using the two-tailed Student's t-test between *Topbp1*<sup>+/+</sup> and *Topbp1*<sup>B5/B5</sup>.

### Enrichment of testes phosphopeptides and TMT labeling

The enrichment of testes phosphopeptides and TMT labeling were done as described previously (Sims et al., 2022 [DOI](#)). Briefly, whole decapsulated testes were collected from 8- to 12-week-old mice after which tissue was subject to lysis, protein quantification and normalization, denaturation, alkylation, precipitation, digestion, and solid-phase extraction (SPE) C18 cartridge clean up as described by Sims et. al (Sims et al., 2022 [DOI](#)). Lyophilized tryptic peptides were then subject to phosphopeptide enrichment using a High-Select Fe-NTA Phosphopeptide Enrichment Kit according to the manufacturer's protocol (Cat# A32992, Thermo Scientific). Phosphopeptide samples were dried in silanized glass shell vials, resuspended in 50 mM HEPES, and labeled with 100 µg of TMT sixplex Isobaric Label Reagents (Thermo Scientific) using 3 TMT channels for each condition (*Topbp1*<sup>+/+</sup> and *Topbp1*<sup>B5/B5</sup>). The TMT-labeling reaction was done at room temperature for 1h and quenched with 5% hydroxylamine for 15 minutes. After quenching, TMT- labeled peptides from all



six channels were pooled, acidified with 0.1% TFA, and desalted using a SPE 1cc C18 cartridge (Sep-Pak C18 cc vac cartridge, 50 mg Sorbent, WAT054955, Waters). Bound TMT-labeled phosphopeptides were eluted with 80% acetonitrile, 0.1% acetic acid in water before being dried via vacuum concentrator.

## Mass spectrometric analysis of TMT-labeled phosphopeptides

The dried TMT-labeled phosphopeptides were prefractionated using offline HILIC HPLC prior to being analyzed by mass-spectrometry as described by Sims et. al (Sims et al., 2022 [\[1\]](#)). The LC-MS/MS was performed on an UltiMate 3000 RSLC nano chromatographic system coupled to a Q-Exactive HF mass spectrometer (Thermo Fisher Scientific). The chromatographic separation was achieved via a 35cm-long 100  $\mu$ m inner diameter column packed in-house with 3  $\mu$ m C18 reversed-phase resin (Reprosil Pur C18AQ 3  $\mu$ m). The Q-Exactive HF was operated in data-dependent mode with survey scans acquired in the Orbitrap mass analyzer over the range of 380–1800 m/z with a mass resolution of 120,000. MS/MS spectra were performed after selecting the top 7 most abundant +2, +3, or +4 ions and a precursor isolation window of 0.7 m/z. Selected ions were fragmented by Higher-energy Collisional Dissociation (HCD) with normalized collision energies of 28, with fragment mass spectra acquired in the Orbitrap mass analyzer with a monitored first mass of 100 m/z, mass resolution of 15,000, AGC target set to  $1 \times 10^5$ , and maximum injection time set to 100 ms. A dynamic exclusion window of 30 seconds was specified.

## Phosphoproteomic data analysis

The Trans Proteomic Pipeline (TPP) version 6.0.0 was used for phosphopeptide identification and quantification. MS data were converted to mzXML using msConvert as packaged with the TPP, after which spectral data files were searched using the Comet search engine (v2021 rev 1) (Eng et al., 2013 [\[2\]](#)). Peptide identifications were validated using PeptideProphet, phosphorylation site localization was performed using PTM Prophet, and TMT channel quantification was performed using Libra. Results from Libra were exported as tab-delimited files for further processing via R scripts as previously described (Sims et al., 2022 [\[1\]](#)). The mass spectrometry phosphoproteomics data have been deposited to the ProteomeXchange Consortium via the PRIDE [1] partner repository with the dataset identifier PXD042199.

## Immunoprecipitation

The immunoprecipitation (IP) experiments were performed as described by Liu et. al (Liu et al., 2017 [\[3\]](#)). Briefly, cell pellets were lysed in 50 mM Tris-HCl, pH 7.5, 150 mM NaCl, 1% tergitol, 0.25% sodium deoxycholate, and 5 mM EDTA, supplemented with EDTA-free protease inhibitor cocktail, 5 mM sodium fluoride, 10 mM  $\beta$ -glycerolphosphate, 1 mM PMSF, and 0.4 mM sodium orthovanadate. The protein extracts were cleared by 10-min centrifugation and then were incubated with anti-FLAG agarose beads (Sigma-Aldrich) for 16h at 4°C. The beads were then washed four times with the same buffer used for IP and then eluted using three resin volumes of the elution buffer (100 mM Tris-HCl, pH 8.0, and 1% SDS, and 1 mM DTT).

## Mass spectrometric analysis of immunoprecipitates

HEK-293T cells were grown in stable isotope labeling with amino acids in cell culture (SILAC) as previously described (Liu et al., 2017 [\[3\]](#)) and transfected as described above. Cells were treated with 1 mM HU for 16h before harvesting. Flag-TOPBP1 was immunoprecipitated using anti-FLAG agarose beads. Immunoprecipitates were then prepared for mass spectrometry analysis by reduction, alkylation, precipitation, and digestion by trypsin. The peptides were desalted, dried, and then fractionated by hydrophilic interaction chromatography as previously described (Liu et al., 2017 [\[3\]](#)). Fractions were dried and analyzed by liquid chromatography–tandem mass spectrometry using a mass spectrometer (Q-Exactive HF Orbitrap; Thermo Fisher Scientific). The capillary column was 35 cm long with a 100- $\mu$ m inner diameter, packed in-house with 3  $\mu$ m C18

reversed-phase resin (Reprosil Pur C18AQ 3  $\mu$ m). Peptides were separated over an 70-minute linear gradient of six to 40% acetonitrile in 0.1% formic acid at a flow rate of 300 nl/min as described previously (Bastos de Oliveira et al., 2015 [DOI](#)). Xcalibur 2.2 software (Thermo Fischer

Scientific) was used for the data acquisition, and The Q-Exactive HF was operated in data-dependent mode with survey scans acquired in the Orbitrap mass analyzer over the range of 380–1800 m/z with a mass resolution of 120,000. The maximum ion injection time for the survey scan was 100 ms with a 3e6 automatic gain-control target ion. Tandem mass spectrometry spectra were performed by selecting up to the 20 most abundant ions with a charge state of 2, 3, or 4 and with an isolation window of 1.2 m/z. Selected ions were fragmented by higher energy collisional dissociation with a normalized collision energy of 28, and the tandem mass spectra was acquired in the Orbitrap mass analyzer with a mass resolution of 17,500 (at m/z 200). The Trans Proteomic Pipeline (TPP) version 6.0.0 was used for peptide identification and SILAC quantification. MS data were converted to mzXML using msConvert as packaged with the TPP, after which spectral data files were searched using the Comet search engine (v2021 rev 1) (Eng et al., 2013 [DOI](#)). The following parameters were used in the database search: semitryptic requirement, a mass accuracy of 15 ppm for the precursor ions, a differential modification of 8.0142 D for lysine and 10.00827 D for arginine, and a static mass modification of 57.021465 D for alkylated cysteine residues. Peptide identifications were validated using PeptideProphet and SILAC quantification was performed using XPRESS as described previously (Bastos de Oliveira et al., 2015 [DOI](#); Sims et al., 2022 [DOI](#)). The mass spectrometry data have been deposited to the ProteomeXchange Consortium via the PRIDE [1] partner repository with the dataset identifier PXD042199.

## Total germ cells preparation

Mice testis were collected from 8- to 12-week-old mice (n = 5 mice, 10 testis for *Topbp1*<sup>+/+</sup>, and n = 20-30 mice, 40-60 testis for *Topbp1*<sup>B5/B5</sup>), and dissociated using standard protocols for germ cell extraction<sup>73</sup>. Briefly, decapsulated testes were held in 10 ml of preheated (35°C) DMEM-F12 buffer containing 2 mg of Collagenase 1A and DNase 7 mg/ml, on a 50 ml conical tube. The collagenase digestion was performed at a 35°C shaker water-bath, 150 rpm during 5 min. The collagenase digestion was stopped by the addition of 40 ml of DMEM-F12 and the tubules were let to decantate for 1 min. The supernatant was removed and added another 40 ml of DMEM-F12 to further wash the residual collagenase and remove somatic and excessive sperm cells. Next, the tubules were digested using 10 ml of DMEM-F12 buffer containing 5 mg of trypsin (Thermo Fisher 27250018) on a 50 ml conical tube and the reaction was carried out on a 35°C shaker water-bath, 150 rpm during 5 min. Digested tubules were strained on a 100  $\mu$ m strainer containing 3 ml of FBS (100% Fetal Bovine Serum, heat inactivated, Sigma F4135-500mL). Total germ cells were centrifuged at 300 xg for 5 min, 4°C and checked for single cells and viability.

## Flow cytometry analysis

Total germ cell extracts were stained with Vybrant dye cycle (VDG) (Invitrogen) 100  $\mu$ M for 30 min at room temperature, kept on dark, and rocking. After staining, cells were sorted as previously described (Rodríguez-Casuriaga et al., 2014 [DOI](#)) aiming to enrich for spermatocytes, and using the Sony MA900 fluorescent activated cell sorter (FACS), tuned to emit at 488 nm and with a 100  $\mu$ m nozzle. Laser power was set to collect VDG-emitted fluorescence in FL1. Sorted cells were collected on 1.5 ml tubes containing 0.5 ml of DMEM-F12 buffer + 10% FBS. The FACS was done at the Flow Cytometry Facility - Cornell University.

## Single-Cell RNA sequencing

Flow sorted cells were submitted to the Cornell DNA Sequencing Core Facility and processed on the 10X Genomics Chromium System targeting 5000–7000 cells per sample as described previously (Grive et al., 2019 [DOI](#)) using the 10X Genomics Chromium Single Cell 3' RNA-seq v2 kit to generate the sequencing libraries, which were then tested for quality control on an ABI DNA Fragment

Analyzer and ran on a NextSeq platform with 150 base-pair reads. The sequencing was carried out to an average depth of 98M reads (range 77M-124M); on average, 91% of reads (range 89%-92%) and then mapped to the reference genome.

## Single-cell RNA sequencing data analysis

Count matrices were generated for each sample using the Cell Ranger counts function and then imported into Seurat and integrated. Cells were filtered based on gene number, UMI, counts, and mitochondrial percentage. Cells with less than 500 genes, less than 1000 UMIs, or more than 5% of mitochondrial reads were excluded from further analysis (Supplemental Figure 29). Raw counts were normalized using Seurat NormalizeData using default parameters and the top 4000 variable features were identified using the FindVariableFeatures function using ExpMean for the mean function and LogVMR for the dispersion function. Principal components were calculated from variable genes and used with Harmony to correct for batch effect. Harmony embeddings dimensions 1-20 were used for a Shared Nearest Neighbor graph with  $k=30$ , unsupervised clustering with a resolution of 4, and Uniform Manifold Approximation and Projection (UMAP) analysis. Cell types were manually identified by use of marker genes, and the SingleR package was used to confirm cell identity. Chromosome X/autosome 9 ratios were calculated by taking the mean gene expression of all genes on chromosome 9 or X for a cell and dividing it by the mean gene expression for all autosomal genes in a cell. Ratios were visualized using ggplot and the introdataviz package geom\_split\_violin function. The single cell heatmap was generated using the DoHeatmap function. The clustered analysis of the X-linked genes shown in **Figure 7A**, was done by splitting the detected 233 X-linked genes into 3 distinct categories based on the difference of RNA level between the spermatocyte stages and normalized by pre-leptotene: reduced silencing ( $> 1$ ), unaltered silencing ( $\geq -1$  or  $\leq 1$ ), or increased silencing ( $< -1$ ). To further split the X-linked genes into 3 categories based on the severity of the silencing defect (detected at spermatocyte 3 stage) in *Topbp1*<sup>B5/B5</sup>: no defect (13 genes), mild (45 genes) or strong defect (170 genes), the difference in expression between SP3 genes from *Topbp1*<sup>+/+</sup> or from *Topbp1*<sup>B5/B5</sup> was calculated. The categories were defined as: Strong  $> 2.5$ , Mild  $\geq 1$  or  $\leq 2.5$  and no defect  $< 1$ . The Single-cell RNAseq data generated in this study have been deposited in the NCBI GEO database under accession number GSE232588.

## Data and code availability

All data and original codes reported in this work, and any additional information required will be shared by the lead contact upon request.

## Acknowledgements

We thank the members of Cohen lab, Weiss lab, Grimson lab and Smolka lab for comments and suggestions. We thank Dr. Fenghua Hu and Dr. Tony Bretscher for the use of the microscopes and Beatriz Almeida for technical assistance. We thank Dr. Lydia Tesfa and the BRC Flow Cytometry Facility (RRID:SCR\_021740) for training and assistance with FACS at the Cornell Institute of Biotechnology, Peter Schweitzer and the BRC Genomics Facility (RRID:SCR\_021727) at the Cornell Institute of Biotechnology for sequencing experiments, Johana M. de la Cruz and the BRC Imaging Facility (RRID:SCR\_021741) at the Cornell Institute of Biotechnology for training and assistance with the Elyra Super Resolution Microscope and the 3D-SIM imaging. We thank Marco Hiler and the BMS and Stem Cell Pathology Unit at the Cornell Veterinary Research Tower for training and assistance with imaging histological sections using ScanScope. We thank Dr. John Schimenti, Dr. Robert Munroe, Mr. Christian Abratte, and Cornell's Stem Cell and Transgenic Core Facility for generating the *Topbp1*<sup>B5/B5</sup> mouse. We thank Dr. Mary Ann Handel for the H1T antibody.

## Author contributions

M.B.S, C.F.R.A and J.R.S. conceived the project. M.B.S and C.F.R.A wrote the paper. C.F.R.A and J.R.S contributed equally with conceptualization, data curation and formal analysis. C.F.R.A, J.R.S and E.A.F. performed experiments. A.D and A.G contributed with data curation and formal analysis. W.C and J.B contributed with data analysis. M.B.S, C.F.R.A, R.W. and P.E.C, contributed with funding acquisition. R.F. contributed with resources.

## Declaration of interests

No competing interests declared.

## Inclusion and diversity

We support inclusive, diverse, and equitable conduct of research.

## Funding

This work was supported by Eunice Kennedy Shriver National Institute of Child Health and Human Development (R01-HD095296) to M.B.S and R.W, National Institute of Health – General Medicine (R35-GM141159) to M.B.S, National Institute of Health (R01HD041012) to P.E.C, the Eunice Kennedy Shriver National Institute of Child Health and Human Development (P50HD104454) to A.G., the Spanish Agencia Estatal de Investigación [PID2019-109222RB-I00/AEI/10.13039/501100011033]; European Union Regional Funds (FEDER) to R. F., and 2022 CVG Scholar Award from the Center of Vertebrates Genomics and the 2022 ASCB International training Scholarship to C.F.R.A.

## References

- Abe H, Alavattam KG, Hu Y-C, Pang Q, Andreassen PR, Hegde RS, Namekawa SH (2020) **The Initiation of Meiotic Sex Chromosome Inactivation Sequesters DNA Damage Signaling from Autosomes in Mouse Spermatogenesis** *Curr Biol* **30**:408–420 <https://doi.org/10.1016/j.cub.2019.11.064>
- Abe H, Alavattam KG, Kato Y, Castrillon DH, Pang Q, Andreassen PR, Namekawa SH (2018) **CHEK1 coordinates DNA damage signaling and meiotic progression in the male germline of mice** *Hum Mol Genet* **27**:1136–1149 <https://doi.org/10.1093/hmg/ddy022>
- Abe H, Yeh Y-H, Munakata Y, Ishiguro K-I, Andreassen PR, Namekawa SH (2022) **Active DNA damage response signaling initiates and maintains meiotic sex chromosome inactivation** *Nat Commun* **13** <https://doi.org/10.1038/s41467-022-34295-5>
- Alavattam KG, Abe H, Sakashita A, Namekawa SH (2018) **Chromosome spread analyses of meiotic sex chromosome inactivation** *Methods in Molecular Biology Humana Press Inc* :113–129 [https://doi.org/10.1007/978-1-4939-8766-5\\_10](https://doi.org/10.1007/978-1-4939-8766-5_10)
- Alavattam KG, Maezawa S, Andreassen PR, Namekawa SH (2022) **Meiotic sex chromosome inactivation and the XY body: a phase separation hypothesis** *Cellular and Molecular Life Sciences* <https://doi.org/10.1007/s00018-021-04075-3>
- Aran D *et al.* (2019) **Reference-based analysis of lung single-cell sequencing reveals a transitional profibrotic macrophage** *Nat Immunol* **20**:163–172 <https://doi.org/10.1038/s41590-018-0276-y>
- Balbo Pogliano C *et al.* (2022) **The CDK1-TOPBP1-PLK1 axis regulates the Bloom's syndrome helicase BLM to suppress crossover recombination in somatic cells** *Sci Adv* **8** <https://doi.org/10.1126/sciadv.abk0221>
- Balmus G *et al.* (2012) **Disease severity in a mouse model of ataxia telangiectasia is modulated by the DNA damage checkpoint gene Hus1** *Hum Mol Genet* **21**:3408–3420 <https://doi.org/10.1093/hmg/dds173>
- Bastos de Oliveira FM, Kim D, Cussiol JR, Das J, Jeong MC, Doerfler L, Schmidt KH, Yu H, Smolka MB (2015) **Phosphoproteomics reveals distinct modes of Mec1/ATR signaling during DNA replication** *Mol Cell* **57**:1124–1132 <https://doi.org/10.1016/j.molcel.2015.01.043>
- Becherel OJ *et al.* (2013) **Senataxin Plays an Essential Role with DNA Damage Response Proteins in Meiotic Recombination and Gene Silencing** *PLoS Genet* **9** <https://doi.org/10.1371/journal.pgen.1003435>
- Bennett CL, La Spada AR, Sattler R, Donnelly CJ (2018) **Senataxin, A Novel Helicase at the Interface of RNA Transcriptome Regulation and Neurobiology: From Normal Function to Pathological Roles in Motor Neuron Disease and Cerebellar Degeneration** *RNA Metabolism in Neurodegenerative Diseases* :265–281 [https://doi.org/10.1007/978-3-319-89689-2\\_10](https://doi.org/10.1007/978-3-319-89689-2_10)
- Bigot N, Day M, Baldock RA, Watts FZ, Oliver AW, Pearl LH (2019) **Phosphorylation-mediated interactions with topbp1 couple 53bp1 and 9-1-1 to control the g1 DNA damage checkpoint** *Elife* **8**:1–28 <https://doi.org/10.7554/eLife.44353>



- Blackford AN, Jackson SP (2017) **ATM, ATR, and DNA-PK: The Trinity at the Heart of the DNA Damage Response** *Mol Cell* **66**:801–817 <https://doi.org/10.1016/j.molcel.2017.05.015>
- Blackford AN, Nieminuszczy J, Schwab RA, Galanty Y, Jackson SP, Niedzwiedz W (2015) **TopBP1 Interacts with BLM to Maintain Genome Stability but Is Dispensable for Preventing BLM Degradation** *Mol Cell* **57**:1133–1141 <https://doi.org/10.1016/j.molcel.2015.02.012>
- Broering TJ, Alavattam KG, Sadreyev RI, Ichijima Y, Kato Y, Hasegawa K, Camerini-Otero RD, Lee JT, Andreassen PR, Namekawa SH (2014) **BRCA1 establishes DNA damage signaling and pericentric heterochromatin of the X chromosome in male meiosis** *J Cell Biol* **205**:663–675 <https://doi.org/10.1083/jcb.201311050>
- Brown EJ, Baltimore D (2000) **ATR disruption leads to chromosomal fragmentation and early embryonic lethality** *Genes and Development* **14** <https://doi.org/10.1101/gad.14.4.397>
- Burgoyne PS, Mahadevaiah SK, Turner JMA (2009) **The consequences of asynapsis for mammalian meiosis** *Nature Reviews Genetics* <https://doi.org/10.1038/nrg2505>
- Carlson M, Falcon S, Pages H, Li N **org. Mm. eg. db: Genome wide annotation for Mouse**
- Carpenter AT (1979) **Recombination nodules and synaptonemal complex in recombination-defective females of *Drosophila melanogaster*** *Chromosoma* **75**:259–292 <https://doi.org/10.1007/BF00293472>
- Cescutti R, Negrini S, Kohzaki M, Halazonetis TD (2010) **TopBP1 functions with 53BP1 in the G1 DNA damage checkpoint** *EMBO J* **29**:3723–3732 <https://doi.org/10.1038/emboj.2010.238>
- Chen Y *et al.* (2018) **Single-cell RNA-seq uncovers dynamic processes and critical regulators in mouse spermatogenesis** *Cell Res* **28**:879–896 <https://doi.org/10.1038/s41422-018-0074-y>
- Cimprich KA, Cortez D (2008) **ATR: An essential regulator of genome integrity** *Nature Reviews Molecular Cell Biology* <https://doi.org/10.1038/nrm2450>
- Cohen S, Puget N, Lin Y-L, Clouaire T, Aguirrebengoa M, Rocher V, Pasero P, Canitrot Y, Legube G (2018) **Senataxin resolves RNA:DNA hybrids forming at DNA double-strand breaks to prevent translocations** *Nat Commun* **9** <https://doi.org/10.1038/s41467-018-02894-w>
- Danielsen JMR, Larsen DH, Freire R, Falck J, Bartek J, Lukas J (2009) **HCLK2 is required for activity of the DNA damage response kinase ATR** *J Biol Chem* **284**:4140–4147
- De Klein A, Muijtjens M, Van Os R, Verhoeven Y, Smit B, Carr AM, Lehmann AR, Hoeijmakers JHJ (2000) **Targeted disruption of the cell-cycle checkpoint gene ATR leads to early embryonic lethality in mice** *Curr Biol* **10** [https://doi.org/10.1016/S0960-9822\(00\)00447-4](https://doi.org/10.1016/S0960-9822(00)00447-4)
- Delacroix S, Wagner JM, Kobayashi M, Yamamoto KI, Karnitz LM (2007) **The Rad9-Hus1-Rad1 (9-1-1) clamp activates checkpoint signaling via TopBP1** *Genes and Development* **21**:1472–1477 <https://doi.org/10.1101/gad.1547007>
- Durinck S, Spellman PT, Birney E, Huber W (2009) **Mapping identifiers for the integration of genomic datasets with the R/Bioconductor package biomaRt** *Nat Protoc* **4**:1184–1191 <https://doi.org/10.1038/nprot.2009.97>

- ElInati E, Russell HR, Ojarikre OA, Sangrithi M, Hirota T, De Rooij DG, McKinnon PJ, Turner JMA (2017) **DNA damage response protein TOPBP1 regulates X chromosome silencing in the mammalian germ line** *Proc Natl Acad Sci U S A* **114**:12536–12541 <https://doi.org/10.1073/pnas.1712530114>
- Eng JK, Jahan TA, Hoopmann MR (2013) **Comet: An open-source MS/MS sequence database search tool** *PROTEOMICS* <https://doi.org/10.1002/pmic.201200439>
- Falck J, Coates J, Jackson SP (2005) **Conserved modes of recruitment of ATM, ATR and DNA-PKcs to sites of DNA damage** *Nature* **434**:605–611 <https://doi.org/10.1038/nature03442>
- Fanning E, Klimovich V, Nager AR (2006) **A dynamic model for replication protein A (RPA) function in DNA processing pathways** *Nucleic Acids Res* **34**:4126–4137 <https://doi.org/10.1093/nar/gkl550>
- Gray S, Cohen PE (2016) **Control of Meiotic Crossovers: From Double-Strand Break Formation to Designation** *Annu Rev Genet* **50**:175–210 <https://doi.org/10.1146/annurev-genet-120215-035111>
- Greenlee AR, Shiao M-S, Snyder E, Buaas FW, Gu T, Stearns TM, Sharma M, Murchison EP, Puente GC, Braun RE (2012) **Deregulated sex chromosome gene expression with male germ cell-specific loss of Dicer1** *PLoS One* **7** <https://doi.org/10.1371/journal.pone.0046359>
- Grive KJ, Hu Y, Shu E, Grimson A, Elemento O, Grenier JK, Cohen PE (2019) **Dynamic transcriptome profiles within spermatogonial and spermatocyte populations during postnatal testis maturation revealed by single-cell sequencing** *PLoS Genet* **15** <https://doi.org/10.1371/journal.pgen.1007810>
- Handel MA, Schimenti JC (2010) **Genetics of mammalian meiosis: regulation, dynamics and impact on fertility** *Nat Rev Genet* **11**:124–136 <https://doi.org/10.1038/nrg2723>
- Hao Y *et al.* (2021) **Integrated analysis of multimodal single-cell data** *Cell* **184**:3573–3587 <https://doi.org/10.1016/j.cell.2021.04.048>
- Hartwell LH, Kastan MB (1994) **Cell cycle control and cancer** *Science* **266**:1821–1828 <https://doi.org/10.1126/science.7997877>
- Hirota T *et al.* (2018) **SETDB1 Links the Meiotic DNA Damage Response to Sex Chromosome Silencing in Mice** *Dev Cell* **47**:645–659 <https://doi.org/10.1016/j.devcel.2018.10.004>
- Holloway JK, Morelli MA, Borst PL, Cohen PE (2010) **Mammalian BLM helicase is critical for integrating multiple pathways of meiotic recombination** *J Cell Biol* **188**:779–789 <https://doi.org/10.1083/jcb.200909048>
- Holloway JK, Sun X, Yokoo R, Villeneuve AM, Cohen PE (2014) **Mammalian CNTD1 is critical for meiotic crossover maturation and deselection of excess precrossover sites** *J Cell Biol* **205**:633–641 <https://doi.org/10.1083/jcb.201401122>
- Ichijima Y, Ichijima M, Lou Z, Nussenzweig A, Daniel Camerini-Otero R, Chen J, Andreassen PR, Namekawa SH (2011) **MDC1 directs chromosome-wide silencing of the sex chromosomes in male germ cells** *Genes and Development* **25**:959–971 <https://doi.org/10.1101/gad.2030811>

- Ichijima Y, Sin HS, Namekawa SH (2012) **Sex chromosome inactivation in germ cells: Emerging roles of DNA damage response pathways** *Cellular and Molecular Life Sciences* <https://doi.org/10.1007/s00018-012-0941-5>
- Inselman A, Eaker S, Handel MA (2003) **Temporal expression of cell cycle-related proteins during spermatogenesis: establishing a timeline for onset of the meiotic divisions** *Cytogenet Genome Res* **103**:277–284 <https://doi.org/10.1159/000076813>
- Jeon Y, Ko E, Lee KY, Ko MJ, Park SY, Kang J, Jeon CH, Lee H, Hwang DS (2011) **TopBP1 deficiency causes an early embryonic lethality and induces cellular senescence in primary cells** *J Biol Chem* **286**:5414–5422 <https://doi.org/10.1074/jbc.M110.189704>
- Jeon Y, Park MK, Kim SM, Bae JS, Lee CW, Lee H (2019) **TopBP1 deficiency impairs the localization of proteins involved in early recombination and results in meiotic chromosome defects during spermatogenesis** *Biochem Biophys Res Commun* **508**:722–728 <https://doi.org/10.1016/j.bbrc.2018.12.001>
- Joshi N, Brown MS, Bishop DK, Börner GV (2015) **Gradual Implementation of the Meiotic Recombination Program via Checkpoint Pathways Controlled by Global DSB Levels** *Mol Cell* **57** <https://doi.org/10.1016/j.molcel.2014.12.027>
- Jung M, Wells D, Rusch J, Ahmad S, Marchini J, Myers SR, Conrad DF (2019) **Unified single-cell analysis of testis gene regulation and pathology in five mouse strains** *eLife* <https://doi.org/10.7554/eLife.43966>
- Kakarougkas A, Ismail A, Katsuki Y, Freire R, Shibata A, Jeggo PA (2013) **Co-operation of BRCA1 and POH1 relieves the barriers posed by 53BP1 and RAP80 to resection** *Nucleic Acids Res* **41**:10298–10311 <https://doi.org/10.1093/nar/gkt802>
- Kassambara A (2019) **Kassambara A. 2019. GGPlot2 Essentials: Great Data Visualization in R. Independently Published.** *GGPlot2 Essentials: Great Data Visualization in R. Independently Published*
- Keeney S, Giroux CN, Kleckner N. (1997) **Meiosis-specific DNA double-strand breaks are catalyzed by Spo11, a member of a widely conserved protein family** *Cell* **88** [https://doi.org/10.1016/S0092-8674\(00\)81876-0](https://doi.org/10.1016/S0092-8674(00)81876-0)
- Khalil AM, Boyar FZ, Driscoll DJ (2004) **Dynamic histone modifications mark sex chromosome inactivation and reactivation during mammalian spermatogenesis** *Proc Natl Acad Sci U S A* **101**:16583–16587 <https://doi.org/10.1073/pnas.0406325101>
- Kolas NK, Svetlanov A, Lenzi ML, Macaluso FP, Lipkin SM, Liskay RM, Greally J, Edelmann W, Cohen PE (2005) **Localization of MMR proteins on meiotic chromosomes in mice indicates distinct functions during prophase I** *J Cell Biol* **171**:447–458 <https://doi.org/10.1083/jcb.200506170>
- Korsunsky I, Millard N, Fan J, Slowikowski K, Zhang F, Wei K, Baglaenko Y, Brenner M, Loh P-R, Raychaudhuri S (2019) **Fast, sensitive and accurate integration of single-cell data with Harmony** *Nat Methods* **16**:1289–1296 <https://doi.org/10.1038/s41592-019-0619-0>
- Kumagai A, Lee J, Yoo HY, Dunphy WG (2006) **TopBP1 activates the ATR-ATRIP complex** *Cell* **124**:943–955 <https://doi.org/10.1016/j.cell.2005.12.041>

- Kwon M, Leibowitz ML, Lee J-H (2020) **Small but mighty: the causes and consequences of micronucleus rupture** *Experimental & Molecular Medicine* <https://doi.org/10.1038/s12276-020-00529-z>
- Lanz MC, Dibitetto D, Smolka MB (2019) **DNA damage kinase signaling: checkpoint and repair at 30 years** *EMBO J* **38** <https://doi.org/10.15252/embj.2019101801>
- Lau X, Munusamy P, Ng MJ, Sangrithi M (2020) **Single-Cell RNA Sequencing of the Cynomolgus Macaque Testis Reveals Conserved Transcriptional Profiles during Mammalian Spermatogenesis** *Dev Cell* **54**:548–566 <https://doi.org/10.1016/j.devcel.2020.07.018>
- Leek JT, Johnson WE, Parker HS, Fertig EJ, Jaffe AE. **sva: Surrogate Variable Analysis R package version 3.10. 0**
- Leimbacher PA *et al.* (2019) **MDC1 Interacts with TOPBP1 to Maintain Chromosomal Stability during Mitosis** *Mol Cell* **74**:571–583 <https://doi.org/10.1016/j.molcel.2019.02.014>
- Lenzi ML, Smith J, Snowden T, Kim M, Fishel R, Poulos BK, Cohen PE (2005) **Extreme heterogeneity in the molecular events leading to the establishment of chiasmata during meiosis I in human oocytes** *Am J Hum Genet* **76**:112–127 <https://doi.org/10.1086/427268>
- Leung CCY, Gong Z, Chen J, Glover JNM (2011) **Molecular basis of BACH1/FANCD1 recognition by TopBP1 in DNA replication checkpoint control** *J Biol Chem* **286**:4292–4301 <https://doi.org/10.1074/jbc.M110.189555>
- Lipkin SM, Wang V, Jacoby R, Banerjee-Basu S, Baxevanis AD, Lynch HT, Elliott RM, Collins FS (2000) **MLH3: a DNA mismatch repair gene associated with mammalian microsatellite instability** *Nat Genet* **24**:27–35 <https://doi.org/10.1038/71643>
- Liu Y, Cussiol JR, Dibitetto D, Sims JR, Twayana S, Weiss RS, Freire R, Marini F, Pelliccioli A, Smolka MB (2017) **TOPBP1Dpb11 plays a conserved role in homologous recombination DNA repair through the coordinated recruitment of 53BP1Rad9** *J Cell Biol* **216**:623–639 <https://doi.org/10.1083/jcb.201607031>
- Manke IA, Lowery DM, Nguyen A, Yaffe MB (2003) **BRCT repeats as phosphopeptide-binding modules involved in protein targeting** *Science* **302**:636–639 <https://doi.org/10.1126/science.1088877>
- Maréchal A, Zou L (2013) **DNA damage sensing by the ATM and ATR kinases** *Cold Spring Harb Perspect Biol* **5** <https://doi.org/10.1101/cshperspect.a012716>
- Marnef A, Legube G (2020) **m6A RNA modification as a new player in R-loop regulation** *Nat Genet* <https://doi.org/10.1038/s41588-019-0563-z>
- Modzelewski AJ, Hilz S, Crate EA, Schweidenback CTH, Fogarty EA, Grenier JK, Freire R, Cohen PE, Grimson A (2015) **Dgcr8 and Dicer are essential for sex chromosome integrity during meiosis in males** *J Cell Sci* **128**:2314–2327 <https://doi.org/10.1242/jcs.167148>
- Modzelewski AJ, Holmes RJ, Hilz S, Grimson A, Cohen PE (2012) **AGO4 regulates entry into meiosis and influences silencing of sex chromosomes in the male mouse germline** *Dev Cell* **23**:251–264 <https://doi.org/10.1016/j.devcel.2012.07.003>

Moens PB, Tarsounas M, Morita T, Habu T, Rottinghaus ST, Freire R, Jackson SP, Barlow C, Wynshaw-Boris A (1999) **The association of ATR protein with mouse meiotic chromosome cores** *Chromosoma* **108** <https://doi.org/10.1007/s004120050356>

Monesi V (1965) **Differential rate of ribonucleic acid synthesis in the autosomes and sex chromosomes during male meiosis in the mouse** *Chromosoma* **17**:11–21 <https://doi.org/10.1007/bf00285153>

Mordes DA, Glick GG, Zhao R, Cortez D (2008) **TopBP1 activates ATR through ATRIP and a PIKK regulatory domain** *Genes and Development* **22**:1478–1489 <https://doi.org/10.1101/gad.1666208>

Nakagawa T, Datta A, Kolodner RD (1999) **Multiple functions of MutS- and MutL-related heterocomplexes** *Proc Natl Acad Sci U S A* <https://doi.org/10.1073/pnas.96.25.14186>

O'Driscoll M (2009) **Mouse models for ATR deficiency** *DNA Repair* **8** <https://doi.org/10.1016/j.dnarep.2009.09.001>

O'Driscoll M, Dobyns WB, Van Hagen JM, Jeggo PA (2007) **Cellular and clinical impact of haploinsufficiency for genes involved in ATR signaling** *Am J Hum Genet* **81** <https://doi.org/10.1086/518696>

Pacheco S *et al.* (2018) **ATR is required to complete meiotic recombination in mice** *Nat Commun* **9** <https://doi.org/10.1038/s41467-018-04851-z>

Parrilla-Castellar ER, Arlander SJH, Karnitz L (2004) **Dial 9–1–1 for DNA damage: the Rad9–Hus1–Rad1 (9–1–1) clamp complex** *DNA Repair* **3**:1009–1014 <https://doi.org/10.1016/j.dnarep.2004.03.032>

Pereira C *et al.* (2022) **Multiple 9-1-1 complexes promote homolog synapsis, DSB repair, and ATR signaling during mammalian meiosis** *Elife* **11** <https://doi.org/10.7554/eLife.68677>

Pereira C, Smolka MB, Weiss RS, Brieño-Enríquez MA (2020) **ATR signaling in mammalian meiosis: From upstream scaffolds to downstream signaling** *Environ Mol Mutagen* **61**:752–766 <https://doi.org/10.1002/em.22401>

Perera D, Perez-Hidalgo L, Moens PB, Reini K, Lakin N, Syväoja JE, San-Segundo PA, Freire R (2004) **TopBP1 and ATR Colocalization at Meiotic Chromosomes: Role of TopBP1/Cut5 in the Meiotic Recombination Checkpoint** *Mol Biol Cell* **15**:1568–1579 <https://doi.org/10.1091/mbc.E03-06>

Reini K, Uitto L, Perera D, Moens PB, Freire R, Syväoja JE (2004) **TopBP1 localises to centrosomes in mitosis and to chromosome cores in meiosis** *Chromosoma* **112** <https://doi.org/10.1007/s00412-004-0277-5>

Rockmill B, Fung JC, Branda SS, Roeder GS (2003) **The Sgs1 helicase regulates chromosome synapsis and meiotic crossing over** *Curr Biol* **13**:1954–1962 <https://doi.org/10.1016/j.cub.2003.10.059>

Rodriguez M, Yu X, Chen J, Songyang Z (2003) **Phosphopeptide binding specificities of BRCA1 COOH-terminal (BRCT) domains** *J Biol Chem* **278**:52914–52918 <https://doi.org/10.1074/jbc.C300407200>



- Rodríguez-Casuriaga R, Santiñaque FF, Folle GA, Souza E, López-Carro B, Geisinger A (2014) **Rapid preparation of rodent testicular cell suspensions and spermatogenic stages purification by flow cytometry using a novel blue-laser-excitable vital dye** *MethodsX* **1**:239–243 <https://doi.org/10.1016/j.mex.2014.10.002>
- Royo H, Polikiewicz G, Mahadevaiah SK, Prosser H, Mitchell M, Bradley A, De Rooij DG, Burgoyne PS, Turner JMA (2010) **Evidence that meiotic sex chromosome inactivation is essential for male fertility** *Curr Biol* **20**:2117–2123 <https://doi.org/10.1016/j.cub.2010.11.010>
- Royo H *et al.* (2013) **ATR acts stage specifically to regulate multiple aspects of mammalian meiotic silencing** *Genes and Development* **27** <https://doi.org/10.1101/gad.219477.113>
- Santos-Pereira JM, Aguilera A (2015) **R loops: new modulators of genome dynamics and function** *Nat Rev Genet* **16**:583–597 <https://doi.org/10.1038/nrg3961>
- Shiloh Y (2003) **ATM and related protein kinases: safeguarding genome integrity** *Nat Rev Cancer* **3**:155–168 <https://doi.org/10.1038/nrc1011>
- Shin Y-H, Choi Y, Erdin SU, Yatsenko SA, Kloc M, Yang F, Jeremy Wang P, Meistrich ML, Rajkovic A (2010) **Hormad1 Mutation Disrupts Synaptonemal Complex Formation, Recombination, and Chromosome Segregation in Mammalian Meiosis** *PLoS Genetics* <https://doi.org/10.1371/journal.pgen.1001190>
- Sims JR *et al.* (2022) **Phosphoproteomics of ATR signaling in mouse testes** *Elife* **11** <https://doi.org/10.7554/eLife.68648>
- Solari AJ (1974) **The behavior of the XY pair in mammals** *Int Rev Cytol* **38**:273–317 [https://doi.org/10.1016/s0074-7696\(08\)60928-6](https://doi.org/10.1016/s0074-7696(08)60928-6)
- Subramanian VV, Hochwagen A (2014) **The meiotic checkpoint network: step-by-step through meiotic prophase** *Cold Spring Harb Perspect Biol* **6** <https://doi.org/10.1101/cshperspect.a016675>
- Svetlanov A, Baudat F, Cohen PE, de Massy B (2008) **Distinct functions of MLH3 at recombination hot spots in the mouse** *Genetics* **178**:1937–1945 <https://doi.org/10.1534/genetics.107.084798>
- Thompson A, Schäfer J, Kuhn K, Kienle S, Schwarz J, Schmidt G, Neumann T, Johnstone R, Mohammed AKA, Hamon C (2003) **Tandem mass tags: a novel quantification strategy for comparative analysis of complex protein mixtures by MS/MS** *Anal Chem* **75**:1895–1904 <https://doi.org/10.1021/ac0262560>
- Turner JMA (2015) **Meiotic Silencing in Mammals** *Annu Rev Genet* **49** <https://doi.org/10.1146/annurev-genet-112414-055145>
- Turner JMA (2007) **Meiotic sex chromosome inactivation** *Development* **134**:1823–1831 <https://doi.org/10.1242/dev.000018>
- Turner JMA, Aprelikova O, Xu X, Wang R, Kim S, Chandramouli GVR, Barrett JC, Burgoyne PS, Deng C-X (2004) **BRCA1, histone H2AX phosphorylation, and male meiotic sex chromosome inactivation** *Curr Biol* **14**:2135–2142 <https://doi.org/10.1016/j.cub.2004.11.032>

- Turner JMA, Mahadevaiah SK, Ellis PJI, Mitchell MJ, Burgoyne PS (2006) **Pachytene asynapsis drives meiotic sex chromosome inactivation and leads to substantial postmeiotic repression in spermatids** *Dev Cell* **10**:521–529 <https://doi.org/10.1016/j.devcel.2006.02.009>
- Vernet N, Mahadevaiah SK, de Rooij DG, Burgoyne PS, Ellis PJI (2016) **Zfy genes are required for efficient meiotic sex chromosome inactivation (MSCI) in spermatocytes** *Hum Mol Genet* **25**:5300–5310 <https://doi.org/10.1093/hmg/ddw344>
- Wang J, Chen J, Gong Z (2013) **TopBP1 controls BLM protein level to maintain genome stability** *Mol Cell* **52**:667–678 <https://doi.org/10.1016/j.molcel.2013.10.012>
- Wang J, Gong Z, Chen J (2011) **MDC1 collaborates with TopBP1 in DNA replication checkpoint control** *J Cell Biol* **193**:267–273 <https://doi.org/10.1083/jcb.201010026>
- Wei T, Simko V (2017) **Wei T, Simko V. 2017. R package “corrplot”: Visualization of a Correlation Matrix (Version 0.84). R package “corrplot”: Visualization of a Correlation Matrix (Version 0.84)**
- Wickham H (2007) **Reshaping Data with the reshape Package** *J Stat Softw* **21**:1–20 <https://doi.org/10.18637/jss.v021.i12>
- Wickham H *et al.* (2019) **Welcome to the tidyverse** *J Open Source Softw* **4** <https://doi.org/10.21105/joss.01686>
- Widger A *et al.* (2018) **ATR is a multifunctional regulator of male mouse meiosis** *Nat Commun* **9** <https://doi.org/10.1038/s41467-018-04850-0>
- Wojtasz L *et al.* (2012) **Meiotic DNA double-strand breaks and chromosome asynapsis in mice are monitored by distinct HORMAD2-independent and -dependent mechanisms** *Genes Dev* **26**:958–973 <https://doi.org/10.1101/gad.187559.112>
- Wojtasz L *et al.* (2009) **Mouse HORMAD1 and HORMAD2, two conserved meiotic chromosomal proteins, are depleted from synapsed chromosome axes with the help of TRIP13 AAA-ATPase** *PLoS Genet* **5** <https://doi.org/10.1371/journal.pgen.1000702>
- Xu Y, Qiao H (2021) **A Hypothesis: Linking Phase Separation to Meiotic Sex Chromosome Inactivation and Sex-Body Formation** *Front Cell Dev Biol* **9** <https://doi.org/10.3389/fcell.2021.674203>
- Yamane K, Wu X, Chen J (2002) **A DNA damage-regulated BRCT-containing protein TopBP1** **1** <https://doi.org/10.1128/MCB.22.2.555-566.2002>
- Yeo AJ, Becherel OJ, Luff JE, Graham ME, Richard D, Lavin MF (2015) **Senataxin controls meiotic silencing through ATR activation and chromatin remodeling** *Cell Discovery* **1** <https://doi.org/10.1038/celldisc.2015.25>
- Zhou ZW, Liu C, Li TL, Bruhn C, Krueger A, Min WK, Wang ZQ, Carr AM (2013) **An Essential Function for the ATR-Activation-Domain (AAD) of TopBP1 in Mouse Development and Cellular Senescence** *PLoS Genet* **9** <https://doi.org/10.1371/journal.pgen.1003702>

## Article and author information

**Carolline F. R. Ascencao**

Department of Molecular Biology and Genetics, Cornell University, United States  
ORCID iD: [0000-0002-0882-7390](https://orcid.org/0000-0002-0882-7390)

**Jennie R. Sims**

Department of Molecular Biology and Genetics, Cornell University, United States  
ORCID iD: [0000-0002-1882-7511](https://orcid.org/0000-0002-1882-7511)

**Alexis Dziubek**

Department of Molecular Biology and Genetics, Cornell University, United States  
ORCID iD: [0000-0002-6621-0700](https://orcid.org/0000-0002-6621-0700)

**William Comstock**

Department of Molecular Biology and Genetics, Cornell University, United States  
ORCID iD: [0000-0002-7977-4679](https://orcid.org/0000-0002-7977-4679)

**Elizabeth A. Fogarty**

Department of Molecular Biology and Genetics, Cornell University, United States

**Jumana Badar**

Department of Molecular Biology and Genetics, Cornell University, United States  
ORCID iD: [0000-0001-5939-8947](https://orcid.org/0000-0001-5939-8947)

**Raimundo Freire**

Fundación Canaria del Instituto de Investigación Sanitaria de Canarias (FIISC), Unidad de Investigación, Hospital Universitario de Canarias, La Laguna, Santa Cruz de Tenerife, Spain, Instituto de Tecnologías Biomédicas, Universidad de La Laguna, 38200 La Laguna, Spain, Universidad Fernando Pessoa Canarias, Las Palmas de Gran Canaria, Spain  
ORCID iD: [0000-0003-4473-8894](https://orcid.org/0000-0003-4473-8894)

**Andrew Grimson**

Department of Molecular Biology and Genetics, Cornell University, United States  
ORCID iD: [0000-0002-5794-6484](https://orcid.org/0000-0002-5794-6484)

**Robert S. Weiss**

Department of Biomedical Sciences, Cornell University, United States  
ORCID iD: [0000-0003-3327-1379](https://orcid.org/0000-0003-3327-1379)

**Paula E. Cohen**

Department of Biomedical Sciences, Cornell University, United States  
**For correspondence:** [mbs266@cornell.edu](mailto:mbs266@cornell.edu)

**Marcus Smolka**

Department of Molecular Biology and Genetics, Cornell University, United States  
**For correspondence:** [mbs266@cornell.edu](mailto:mbs266@cornell.edu)  
ORCID iD: [0000-0001-9952-2885](https://orcid.org/0000-0001-9952-2885)

## Copyright

© 2023, Ascencio et al.

This article is distributed under the terms of the [Creative Commons Attribution License](#), which permits unrestricted use and redistribution provided that the original author and source are credited.

## Editors

Reviewing Editor

**Akira Shinohara**

Osaka University, Suita/Osaka, Japan

Senior Editor

**Wei Yan**

University of California, Los Angeles, Torrance, United States of America

### Reviewer #1 (Public Review):

This is a very well-written and performed study describing a TOPBP1 separation of function mutation, resulting in defective MSCI maintenance but normal sex body formation. The phenotype differs from that of a previous TOPBP1 null allele, in which both MSCI and sex body formation were defective. Additional defects in CHK phosphorylation and SETX localization are also described.

Strengths:

The study is very rigorous, with a remarkably large number spectrum of techniques deployed to support the conclusions

Weaknesses

The study claims that MSCI is initiated but not maintained in the mutant. I think alternative hypotheses are possible.

<https://doi.org/10.7554/eLife.90887.2.sa2>

### Reviewer #2 (Public Review):

Summary:

This paper described the role of BRCT repeat 5 in TOPBP1, a DNA damage response protein, in the maintenance of meiotic sex chromosome inactivation (MSCI). By analyzing a Topbp1 mutant mouse with amino acid substitutions in BRCT repeat 5, the authors found reduced phosphorylation of a DNA/RNA helicase, Sentaxin, and decreased localization of the protein to the X-Y sex body in pachynema. Moreover, the authors also found decreased repression of several genes on the sex chromosomes in the male mice.

Strengths:

The works including phospho-proteomics and single-cell RNA sequencing with lots of data have been done with great care and most of the results are convincing.

Weaknesses:

No weakness.

<https://doi.org/10.7554/eLife.90887.2.sa1>

### Reviewer #3 (Public Review):

The work presented by Ascencio and coworkers aims to deepen into the process of sex chromosome inactivation during meiosis (MSCI) as a critical factor in the regulation of meiosis progression in male mammals. For this purpose, they have generated a transgenic mouse model in which a specific domain of TOPBP1 protein has been mutated, hampering the binding of a number of protein partners and interfering with the regulatory cascade initiated by ATR. Through the use of immunolocalization of an impressive number of markers of MSCI, phosphoproteomics and single cell RNA sequencing (scRNAseq), the authors are able to show that despite a proper morphological formation of the sex body and the incorporation of most canonical MSCI makers, sex chromosome-linked genes are reactivated at some point during pachytene and this triggers meiosis progression breakdown, likely due to a defective phosphorylation of the helicase SETX.

The manuscript presents a clear advance in the understanding of MSCI and meiosis progression with two main strengths. First, the generation of a mouse model with a very uncommon phenotype. Second, the use of a vast methodological approach. The results are well presented and illustrated. Nevertheless, the discussion could be still a bit tuned by the inclusion of some ideas, and perhaps speculations, that have not been considered.

<https://doi.org/10.7554/eLife.90887.2.sa0>

### Author Response

The following is the authors' response to the original reviews.

#### Public Reviews:

##### Reviewer #1 (Public Review):

###### Summary:

*This is a very well written and performed study describing a TOPBP1 separation of function mutation, resulting in defective MSCI maintenance but normal sex body formation. The phenotype differs from that of a previous TOPBP1 null allele, in which both MSCI and sex body formation were defective. Additional defects in CHK phosphorylation and SETX localization are also described.*

###### Strengths:

*The study is very rigorous, with a remarkably large number of MSCI marks assayed, phosphoproteomics (leading to the interesting SETX discovery) and 10X RNAseq, allowing the MSCI phenotype to be further deconvolved. The approaches in most cases are robust.*

###### Weaknesses:

*There aren't many; please find list below:*

- 1. The authors are committed to the idea that maintenance of MSCI is the major defect here. However, based on the data, an alternative would be that some cells achieve sex body formation and MSCI normally, while others do not. It would only take a small percentage of cells exhibiting MSCI failure to kill all the cells in the same germinal epithelium, so this could still explain the complete pachytene block. This isn't a major point...this phenotype is clearly different to the TOPBP1 KO, but a broader discussion of possibilities in the discussion would help. I raise this in the context of both the cytology and 10X analysis:*

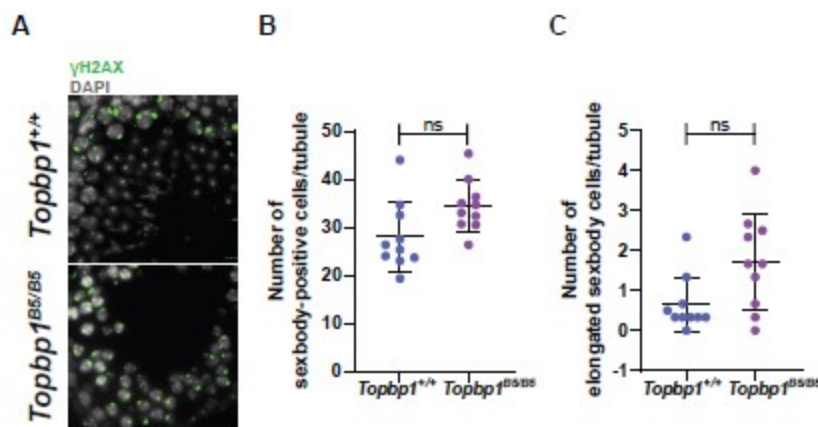


*a) The assessment that sex body formation is normal is based on cytology in Supp 8 and 9, but a more rigorous approach would be to assess condensation of the XY pair in stage-matched spread cells (maybe they have that data already) by measuring distances between the X and Y centromere, or looking at stage IV of the seminiferous cycle, where all cells should have oval sex bodies but sex body mutants have persistent elongated XY pairs (see work of Namekawa and Turner). The authors do actually mention that γH2AX spreading is defective in many cells....and if this is true, condensation to form a sex body would almost certainly not have taken place in those cells.*

We appreciate the reviewer's comment and have performed the experiment suggested, counting the number of elongated sex bodies in all sex body-positive cells in seminiferous tubules stained with γH2AX and DAPI (as done by Turner in Hirota et al., 2018). The experiment did not show significant differences between *Topbp1*<sup>+/+</sup> and *Topbp1*<sup>B5/B5</sup> as shown in Author response image 1.

#### Author response image 1.

*Topbp1*<sup>B5/B5</sup> displays normal condensation of the XY-pair. A) Immunostaining of XY condensation in *Topbp1*<sup>+/+</sup> and *Topbp1*<sup>B5/B5</sup> testes sections (γH2AX: green and DAPI: gray). B) Quantification of all sex body-positive cells per tubule (*Topbp1*<sup>+/+</sup> number of cells counted = 781, number of tubules counted = 28, number of mice = 3; *Topbp1*<sup>B5/B5</sup> number of cells counted = 967, number of tubules counted = 28, number of mice = 3). C) Quantification of elongated-sex body cells per tubule (*Topbp1*<sup>+/+</sup> number of cells counted = 19 and 762 normal round/oval-sex bodies cells, number of tubules counted = 28, number of mice = 3; *Topbp1*<sup>B5/B5</sup> number of cells counted = 45 and 922 normal round/oval-sex bodies cells, number of tubules counted = 28, number of mice = 3).



*b) Regarding the 10X data, the finding that expression of some XY genes is elevated and others are not is also consistent with a "partial" phenotype (some cells have normal XY bodies and MSCI, others fail in both). In Fig 6E, X expression looks to be elevated in B5 vs wt at all stages...if this were a maintenance issue, shouldn't it be equal to that in wt and then elevate later?*

We understand the point raised by the reviewer, however we do not favor the "partial" phenotype model because of the absence of any post-pachytene spermatocytes in the B5 mutant. If some cells had escaped the MSCI defect, we would expect to detect cells progressing further in meiosis. Because we cannot rule out completely the possibility of a subtle disruption in XY silencing initiation, we decided to better emphasize this point in the discussion (lines 391-394).

In Figure 6E, the X-linked genes were normalized against chromosome 9-linked genes. The normalization against pre-leptotene was done for the results displayed on Figure 7, in which we demonstrate the maintenance issue. Furthermore, for the 10X analysis, while the same number of cells were loaded for wild-type and mutant, the composition of cells varied between these two samples. Despite the fact that very few “spermatocyte 3” cells were detected in the mutant, those cells displayed much higher X-linked gene expression than the wild-type spermatocyte 3 cells.

*1. How is the quantitation showing impaired localization of select markers (e.g. SETX) normalized? How do we know that the antibody staining simply didn't work as well on the mutant slides?*

The quantification showing impaired localization of the selected markers such as SETX was done as described by Sims, et al. 2022 and Adams, et al. 2018. In brief, the green signal was measured along (XY cores) or across (XY DNA loops) the X and Y chromosomes and normalized against the analogous signal on the autosomal chromosomes. The possibility that the antibody simply did not work as well on the mutant is unlikely since multiple biological replicates were performed and we reproducibly followed standard practices in the field for meiotic spreads staining, imaging, and quantification. We also note that our findings published in Sims et al, 2022 show that ATR inhibition strongly impairs SETX localization to the sex body, further substantiating our claim that signaling via ATR-TOPBP1 controls SETX.

*1. Is testis TOPBP1 protein expression reduced in the B5 mutant?*

TOPBP1 protein abundance in the B5 mutant is reduced in lysates from whole testis, measured via western blot. We did not detect a significant reduction in TOPBP1 signal intensity measured by immunofluorescence in pachytene spreads of the B5 mutant.

*1. 10X analysis: how were the genes on the y-axis in Supp 24 arranged? Is this by location on the X chromosome?*

These genes were sorted by location across the chromosome X.

*1. The final analyses in Fig 7: X-genes are subdivided based on their behavior (up, down, unchanged). What isn't clear to me is whether the authors have considered the fact that there are global changes in gene expression during meiosis (very low in lep , zyg and early pach, then ramps up hugely from mid pach). In other words, is this normalized to autosomal gene expression?*

For the final analysis in Fig7, the normalization was done by their expression at the pre-leptotene stage. Moreover, the analysis was made comparing X-linked gene behavior in Wild-type vs B5 mutant.

*1. Again regarding the 10X analysis, my prediction would be that not ALL X and Y gene would increase in pach if MSCI were ablated...we should remember that XY genes have been subject to MSCI for some 160 million years of evolution, and this will mean that many enhancers that originally drove their expression prior to the evolution of MSCI will now be lost. This has been our experience: many XY genes aren't elevated at pach even in mutants in which MSCI is totally defective. I'd urge the authors to consider this possibility when they use XY gene expression patterns to diagnose the severity or timing of the MSCI phenotype. This could be a discussion point.*

We greatly appreciate the reviewer's suggestion and have added discussion about this point to lines 392400).

**Reviewer #2 (Public Review):**

*Summary:*

*This paper described the role of BRCT repeat 5 in TOPBP1, a DNA damage response protein, in the maintenance of meiotic sex chromosome inactivation (MSCI). By analyzing a Topbp1 mutant mouse with amino acid substitutions in BRCT repeat 5, the authors found reduced phosphorylation of a DNA/RNA helicase, Sentaxin, and decreased localization of the protein to the X-Y sex body in pachynema. Moreover, the authors also found decreased repression of several genes on the sex chromosomes in the male mice.*

*Strengths:*

*The works including phospho-proteomics and single-cell RNA sequencing with lots of data have been done with great care and most of the results are convincing.*

*Weaknesses:*

*One concern is that, although the Topbp1 mutant spermatocytes show very severe defects after the stage of late pachynema, the defect in the gene silencing in the sex body is relatively weak. It is a bit difficult to explain how such a weak mis regulation of the gene silencing in mice causes the complete loss of cells in the late stage of spermatogenesis.*

We appreciate the reviewer's comment. We note that even subtle mis-regulation of XY gene silencing has been reported to lead to significant loss of cells in late stage of prophase I (Ichijima et al., 2011; Modzelewski et al., 2012). Moreover, it is possible that some cells with drastic changes in X-gene expression were excluded from the downstream analysis due to high levels of mitochondrial gene expression (cells that were likely dying due to apoptosis). The exclusion of cells with high levels of mitochondrial gene expression is a common practice in downstream analysis of sc-RNA sequencing data.

**Reviewer #3 (Public Review):**

*The work presented by Ascencio and coworkers aims to deepen into the process of sex chromosome inactivation during meiosis (MSCI) as a critical factor in the regulation of meiosis progression in male mammals. For this purpose, they have generated a transgenic mouse model in which a specific domain of TOPBP1 protein has been mutated, hampering the binding of a number of protein partners and interfering with the regulatory cascade initiated by ATR. Through the use of immunolocalization of an impressive number of markers of MSCI, phosphoproteomics and single cell RNA sequencing (scRNAseq), the authors are able to show that despite a proper morphological formation of the sex body and the incorporation of most canonical MSCI makers, sex chromosome-linked genes are reactivated at some point during pachytene and this triggers meiosis progression breakdown, likely due to a defective phosphorylation of the helicase SETX.*

*The manuscript presents a clear advance in the understanding of MSCI and meiosis progression with two main strengths. First, the generation of a mouse model with a very uncommon phenotype. Second, the use of a vast methodological approach. The results are well presented and illustrated. Nevertheless, the discussion could be still a bit tuned by the inclusion of some ideas, and perhaps speculations, that have not been considered.*

We appreciate the reviewer's comment and have improved the discussion section addressing the points raised in the "recommendation For the Authors".

**Reviewer #1 (Recommendations For The Authors):**

*I don't have any additional points here*

**Reviewer #2 (Recommendations For The Authors):**

*The paper by Ascencio et al. describes a separation-in-function allele of TOPBP1 critical for DNA damage response (DDR) that confers a specific defect in XY sex chromosome inactivation during male mouse meiosis. The authors constructed a Topbp1 separation-of-function mouse by introducing amino acid substitutions in BRCT repeat 5 and found the mice with normal DDR response in mitosis and meiosis show male infertility. Topbp1(B5/B5) mice do not contain spermatocytes after diplotene, as a result, little spermatids/sperms. In the mice, most of the meiotic events in prophase I including chromosome synapsis and meiotic recombination as well as the formation of the sex body are normal. The detailed proteomic analysis revealed the reduced ATR-dependent phosphorylation of a DNA/RNA helicase, Sentaxin. And also single-cell RNA sequencing found that the expression of some of genes from sex chromosomes are not silenced well compared to the control. The works with lots of data have been done with great care and most of the results are convincing. One clear concern is that, although the authors nicely showed a defect in gene silencing in sex chromosomes in the Topbp1(B5/B5) mice, how a small defect in the gene silencing leads to the complete loss of diplotene spermatocytes remains unaddressed.*

*Major points:*

*Although the authors showed a change in the transcriptome in spermatocytes of Topbp1(B5/B5) male mice, the authors cannot explain the complete lack of spermatids in this mouse. Even the transcriptome seems not to provide a clue.*

- 1. Given that the TOPBP1-B5 protein cannot bind to both 53BP1 and BLM, it is interesting to check the localization of both proteins on meiotic chromosome spreads (in the case of 53BP1, the localization in MEFs with DNA damage).*

We appreciate the reviewer's comment. We have tried to stain BLM in meiotic spreads using several different antibodies, however we were not successful getting specific signals for BLM. In the case of 53BP1, we monitored its localization, and it was not significantly different from Topbp1<sup>-/-</sup> meiotic spreads, please refer to Supplemental Figure 11. While we appreciate the reviewer's suggestion of looking at the localization of 53BP1 in MEFs with DNA damage, we opted not to perform the experiment because we have shown that 53BP1 can still bind the BRCT 1 and 2 domains of TOPBP1 as previously described (Bigot et al., 2019; Cescutti et al., 2010; Liu et al., 2017). Additionally, both male and female 53BP1 KO mice are fertile (Ward et al., 2003), thus the partial disruption in binding to 53BP1 that we observed in TOPBP1 B5 mutant is likely not causing the infertility phenotype.

- 1. A recent preprint by Fujiwara et al. (doi: <https://doi.org/10.1101/2023.04.12.536672>) showed the accumulation of R-loops in spermatocyte spreads in Senataxin knockout mice. The authors may check the R-loop on the sex body in Topbp1-B5 mice.*

We thank the reviewer for the suggestion. We have tried several protocols to stain R-loops (including the protocol used in the paper mentioned above) but were not successful.

1. The authors need to check the protein level (and band shift) of Senataxin in the testis by western blotting analysis.

We have tried several SETX antibodies, and none worked for western blot analysis.

1. If possible, the authors can see any protein interaction between TOPBP1 and Senataxin.

We appreciate the suggestion, and we will investigate this interaction in future work.

1. The authors need to check the statistics in the paper.

(1) It is better to show actual P-values in the case of "ns".

P-values were added to the respective figure legends.

(2) In focus counting such as Figures 3D, G, H, 4B, D, F, H, 5E, and F (and in Supplemental Figures), please indicate how many spreads were counted in each mouse. Moreover, the distribution of focus numbers and intensity of fluorescence are not parametric (not normal distribution). It is better to use a non-parametric method such as Mann-Whitney's U test.

We appreciate the reviewer's comment and upon consulting with a Statistician at Cornell Statistical Consulting Unit (CSCU), we were advised to use a linear mixed effect model to take into account the variability in cells within each mouse when comparing mice between groups (Topbp1<sup>+/+</sup> vs Topbp1B5/B5). We then reanalyzed all quantified meiotic spreads using this mixed effect model, and the p-value, number of mice, and number of cells counted for each group are displayed in the respective figure legends. Upon going through all the quantified meiotic spreads, we realized a minor error in one of the previous data points related to SETX staining in Topbp1<sup>+/+</sup> and have fixed it. Using the previous quantification data and the new stats analysis the p-value for cores was 0.5598 and \*p-value for loops was 0.0273. Now using the correct values and the new stats analysis the p-value for cores is 0.5987 and \*p-value for loops is 0.0452. The correction did not change the conclusion of this data and is now displayed in the new Figure 5. We also realized a mistake in the ATR quantification when the spreadsheet was moved from excel to Graphpad. Using the previous quantification and the new stats analysis the p-value for cores was 0.2451 and p-value for loops was 0.8933. Now using the correct values and the new stats analysis the p-value for cores is 0.4068 and p-value for loops is 0.9396. The correction did not change the conclusion of this data and is now displayed in the new Figure 4. Moreover, we realized that we used n = 8 (n = number of mice) for MDC1 quantification and n = 2 for pCHK1\_S345, instead of n = 3 as shown in the preprint version of the manuscript. Corrected values were added to their respective figures and figure legends.

(3) From Figures 6E, 7B, and 7C, the authors conclude the difference in the expression profile between wild type and Topbp1(B5) spermatocytes. It is better to show P-values for the comparison. Particularly, in Figure 7C, Xiap expression kinetics look similar between wild type and the mutant.

We have added p-values to figures 6E and 7B and their respective figures or figure legends. In figure 7C, we now recognize that the  $\Delta$  could have been misleading as we meant to compare Wild-type SP2 to Wild-type SP3 and Mutant SP2 to SP3; and not comparing Wild-type SP3 to Mutant SP3. Therefore, the  $\Delta$  was excluded from Figure 7C. For the comparisons between expression levels of SP2 and SP3, it is challenging to calculate p-values for a single gene since these cells have started X-gene silencing and expression values are very low. Meaningful p-values for the comparisons between Wildtype SP3 to Mutant SP3 can be

visualized in Figure 7B, where the comparison is based on number of genes instead of expression levels of each gene.

*Minor comments:*

1. Line 34: *SPO11 is NOT a nuclease. Just delete it.*

It has been deleted (see line 34).

1. Line 71, a protein: *Is this protein ATR? If so, please write it. If not, please give the name of the protein.*

In line 71 (now lines 79-80), we refer to TOPBP1-interacting proteins in general since many of these interactions happen through a phosphorylation in the TOPBP1's interactor. This is the case for BLM, 53BP1, FANCD1, and RAD9. ATR interacts with TOPBP1 through TOPBP1's AAD domain and this is not a phospho-mediated interaction. We restructured the sentence for clarity.

1. In the Introduction, the authors often refer to a review by Cimprich and Cortez (2008) in various places. *It is better to cite an original paper or the other an appropriate review.*

We have accepted the reviewer's suggestion and added original papers when appropriate.

1. Line 143-145: *The authors generated eight charge reversal point mutations in the BRCT domain 5 of TOPBP1. If possible, it is helpful to mention the logic to generate these substitutions and also why BRCT domain 5, is not other domains.*

We generated eight charge reversal point mutations to abrogate all possible phospho-dependent interactions and avoid potential residual interactions. We have mutated other BRCT domains as well, which will be published separately.

1. Line 174 (and Figure 2E): *RPA should be either RPA2 or RPA32.*

Corrected (it is RPA2).

1. Figure 5C-F: *Please explain in more detail how the authors quantified the SETX signals. Why the two results are different?*

The quantification was done as described by Sims, et al. 2022, yielding separate data for XY cores and DNA loops. In brief, the green signal was measured along (XY cores) or across (XY DNA loops) the X and Y chromosomes. Signals were normalized by the signal in the autosomal chromosomes.

**Reviewer #3 (Recommendations For The Authors):**

*I have no major criticisms, but I include a list of comments and suggestions (some of them conceptual, and disputable) that could help the authors to improve some parts of the manuscript.*



1. Line 52: I realize that the term protein "sequestration" (used in many instances along the manuscript) has been widespread in the literature related to MSCI in the last years. While this might be a cool way to describe the dynamics of proteins accumulating in the sex body, this reviewer considers this term is totally inappropriate. It is confusing and introduces at least to mistakes to the fact of protein accumulation in the sex body. First, it seems to indicate that once trapped in the sex body, proteins are incapable of leaving it, which might be completely wrong (histone replacement refutes this idea). Second, it is suggested that DDR proteins are attracted by the sex body and cannot remain associated to autosomes even if DNA repair has not been completed. This has also been demonstrated to be incorrect (see for example PDMI 19714216). Moreover, DDR proteins can associate *de novo* to chromosomes if needed, for instance upon DNA damage caused by chemicals or irradiation. Thus, I suggest that the use of "sequestration" should be evaluated more critically, evaluating the misleading ideas that are subjacent to this term. The use of protein "accumulation" is much more objective and descriptive of the real facts.

We thank the reviewer's suggestion and have addressed it in lines 52, 97 and 324.

1. Line 88: Just as a deference to the original ideas, it would be nice to acknowledge that the inactivation of sex chromosomes and the formation of a sex body in mouse meiosis was described more than 50 years ago (PDMI 5833946; 4854664). Likewise, the ideas about the sequential achievement and reinforcement of MSCI during pachytene have been developed during the last 20 years, far before the recent reports cited in the manuscript. Citations to these "old fashion" works would be great.

We appreciate the reviewer's suggestion and have addressed it in line 86.

1. Line 90. Please, take into consideration that such a strong effect on meiosis progression occurs mainly in some knockout mice models and that in many other models (including hybrid mice models from natural populations) autosomal regions can remain unsynapsed and accumulate DDR proteins without impairing meiosis. In other mammalian species, meiosis is even more permissive to these MSUC phenomena.

We appreciate the reviewer's suggestion and have addressed it at line 88.

1. Line 211: The differences in the abundance of MLH1 and MLH3 are remarkable. If these two proteins are supposed to form a heterodimer leading to crossover formation, then the increase of only MLH1 might be related to a different process, not leading to crossover (even not class II ones).

We agree with the reviewer's comment and have included this point in the discussion (lines 491- 497).

1. Line 217: I have some doubts about the results presented in Supplementary Figure 9. First, it is not clear to me how the represented cells counts were performed. Each spot is supposed to represent cell counts in a single individual, but how many cells were counted per individual? The proportion of cells could be a better indicator. Second, some B5/B5 individuals' counts were close to the ones displayed in the wild type. Did mutant animals show a high divergence compared to each other? It could be great to have each individual data displayed in a pie chart, and not only the aggregated data.

We have now addressed this in the new Supplemental figure 9 legend. Each dot in the graph represents the sum of cells counted for each individual. We counted cells from 8 mice for each, *Topbp1*<sup>+/+</sup> and *Topbp1*<sup>B5/B5</sup>.

Here we summarize the total cells counted per individual:

**Author response table 1.**

Mouse	<i>Topbp1</i> <sup>+/+</sup>	<i>Topbp1</i> <sup>B5/B5</sup>
1	26	43
2	46	72
3	43	84
4	79	64
5	37	29
6	48	52
7	74	67
8	52	8

1. Line 222: The data on 53BP1 deserve further attention. On the one side, from the analysis presented in Supplementary Figure 11, it seems that 53BP1 tends to show a lower intensity in *Topbp1*<sup>B5/B5</sup> mice. Since only 2 mice were analyzed, while for most of the other proteins 3-8 animals were studied, I suggest increasing the number of animals analyzed for 53BP1 localization, to test if this slight difference turns significant. This is relevant since: 1) the association of 53BP1 protein in somatic cells was clearly affected, and 2) 53BP1 is one of the last MSCI markers incorporated to the sex body at mid-late pachytene. These results should be moved to the main text and not appear as supplementary data. On the other hand, if no differences were to be found in meiosis, compared to somatic cells, how do authors explain these differences? Would 53BP1 have another partner at the sex body apart from TOPBP1? Could TOPBP1 have other BRCT domains (apart from domain 5) able to bind 53BP1?

We appreciate the reviewer's suggestion; however, we had an issue with 53BP1 antibody. We analyzed 2 mice and needed to re-order the antibody. This antibody was backordered for almost one year, and when we finally received the order, the company had changed the clone for this antibody, and it no longer worked for meiotic spreads. In somatic cells, we see in HEK-293T a partial disruption in the binding to TOPBP1 B5 through IP-MS and IP-Western blot. The disruption is only partial due to the binding of 53BP1 to other domains in TOPBP1 such as BRCT 1 and 2 (Bigot et al., 2019; Cescutti et al., 2010; Liu et al., 2017). However, in assays in which we would expect a phenotypic response caused by impaired 53BP1, we did not see any effect, such as survival after IR (using the mice) and survival after phleomycin challenge (using Mefs). Moreover, 53BP1 KO mice, males and females, are fertile (Ward et al., 2003) so, the partial disruption in binding to 53BP1 that we observed in TOPBP1 B5 mutant is likely not causing the infertility phenotype.

1. Line 250: I do not understand what is represented in Figure 5A. Why did the author mix two different experiments (differences in phosphoprotein abundance in B5/B5 compared to wild type and the interference of ATR with AZ20)?

To account for the differences in cell population observed in the whole testis between Topbp1<sup>+/+</sup> and Topbp1B5/B5, and to know exactly which phosphorylation changes were due to disruption in the ATR signaling and not pleiotropic effects, we combined two different phosphoproteomes: One phosphoproteome from the comparison between Topbp1<sup>+/+</sup> and Topbp1B5/B5 and another one from the comparison between Vehicle or ATR inhibitor-treated mice. By utilizing this approach, we only consider hits that were disrupted in both analyses. A similar method was used by Sims et.al, 2022 (Sims et al., 2022).

1. It is not clearly explained what is represented in Figure 6B. There is no explanation in the text or the figure legend. Do this represent the difference between scRNAseq in control and Topbp1B5/B5? If so, please, clarify.

We thank the reviewer's comment and have addressed it in the legend of Figure 6B.

1. Line 342 and following. The authors describe a decrease of gene silencing. The use of two negative concepts is always confusing and results in the conversion to a positive one. I suggest considering the possibility of just talking about increase of gene expression, in order to make the message clearer.

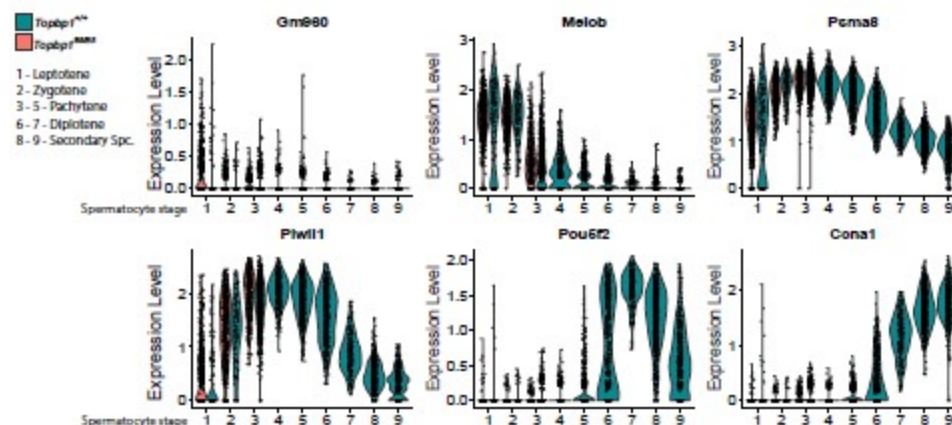
We appreciate the reviewer's point here, but it is important to note that the phenomenon disrupted in our mutants is MSCI, which is by definition a gene silencing mechanism. This phenotype is not as simple as "increased gene expression", it is the removal of a mechanism that is a key feature of prophase I. Thus, because we are focusing on the mechanism of MSCI, it is crucial to maintain this (albeit unusual) terminology.

1. As for the classification of spermatocytes into 9 categories, I am curious about which spermatocytes are included in each of these categories. For instance, from cytology it seems that in Topbp1B5/B5 mice, spermatocytes are able to reach mid-late pachytene. However, in the spermatocyte categories established by scRNAseq they only reach class 3. Therefore, which are the populations included in the remaining 6 classes of spermatocytes? Do authors have any morphological correlation to these scRNAseq categories? Is it possible that in this mutant morphological advance of meiosis and gene expression profiles are uncoupled?

The clustering of cells to a specific group is based on RNA expression, which does not always match cytological features. Moreover, during the analysis, cells with high expression of mitochondrial genes are excluded (these are dying cells that do not pass the quality control). Thus, while Topbp1B5/B5 reaches a mid-late-pachytene stage according to cytological analyses, in the single-cell RNA seq analysis we could only detect one pachytene stage. The other 6 remaining categories of spermatocytes can be classified according to their best-fit profile of gene expression. For that, we use the classification described by Chen et al., 2018 and Lau et al., 2020. Spermatocytes 3-5 = Pachytene, Spermatocytes 6-7 = Diplotene, Spermatocytes 8-9 = secondary spermatocytes (metaphase I/II). The gene markers used for this classification are displayed in Author response image 2.

#### Author response image 2.

Genes used as markers of spermatocytes captured in the scRNAseq analysis. Violin plots display the distribution of cells expressing Gm960 (Leptotene marker), Meiob (Leptotene/Zygotene marker), Psma8 (Pachytene marker), Pwill1 (Pachytene marker), Pou5f2 (Diplotene marker), and Ccna1 (Secondary Spermatocytes marker).



1. Figure 6E shows that overexpression of X-linked genes is not a feature of spermatocytes but it is initiated in spermatogonia. This fact has not been properly stated in the text and perhaps not sufficiently highlighted.

We noticed subtle changes during the spermatogonia stage and have addressed the reviewer's comment in lines 317-322, however the downstream analyses related to a defect in X-gene silencing maintenance displayed in Figure 7 were done based on normalization of gene expression to its respective pre-leptotene stage.

1. Supplementary Figure 24 shows that some X-linked genes are more expressed in Topbp1B5/B5 compared to control mice. In the figure it can be observed that many genes accumulate at the bottom of the graph. Does this have any correlation to the location of these genes along the X chromosome, for instance near or within the PAR? This could correlate with the defects in  $\gamma$ H2AX accumulation at this region.

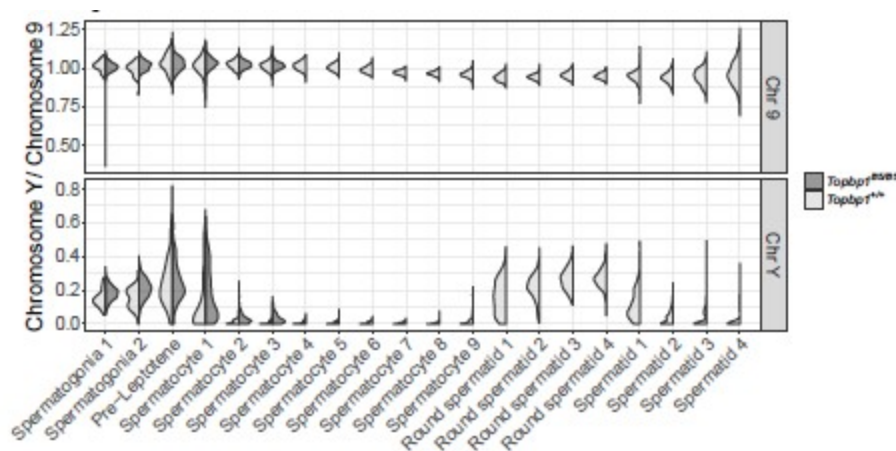
These are the locations along the chromosome. Only the bottom 5 rows are within the PAR region, so this accumulation is not within the PAR region specifically. The bottom tenth of the genes in the heatmap correspond to roughly a 17 Mb region.

1. The authors only analyzed the overexpression of genes located on the X chromosome. It would be interesting to show the behavior of Y-linked genes as well.

The coverage of Y-linked genes was not very high and that is why we have not shown the results in the paper. However, the results for Y-linked genes were similar to the X-linked genes and can be visualized in Author response image 3.

### Author response image 3.

Single cell RNAseq reveals that Topbp1B5/B5 spermatocytes initiate MSCI but fail to promote full silencing of Y chromosome-linked genes. Violin plot displaying the ratio of the average expression of Y chromosome genes by the average expression of chromosome 9 genes at different stages of spermatogenesis for Topbp1+/+ and Topbp1B5/B5 cells.



1. Line 425: Authors indicate that it is not known if association of TOPBP1 and BLM, 53BP1 or other proteins is disrupted in Topbp1B5/B5 spermatocytes. Could these experiments be performed in the testis, as they were in somatic cells?

The cellular composition in Topbp1+/+ and Topbp1B5/B5 testes is very different so it would not be a fair comparison. While we have tried to isolate pachytene cells to perform these experiments, we were successful only when using Topbp1+/+ but not Topbp1B5/B5, likely due to the extremely small size of the mutant testis.

1. Line 455 and following. I find that the discussion about the role of SETX is not completely clear. It seems that a failure of SETX function could result in defective or no transcription, as a consequence of the impossibility to resolve RNA-DNA hybrid molecules. Therefore, should impairment of SETX lead to reduced or enhanced transcription? Please clarify. On the other hand, this defect in SETX function should affect the whole genome, and not only sex chromosomes. Do authors have any clues about this broad effect?

We thank the reviewer's comment and have expanded on discussion in lines 470-474. While we agree with the reviewer's point that an impairment on SETX should affect the whole genome, however, during pachytene stage, SETX is mostly localized to the sex body. The Topbp1B5/B5 shows a specific defect in X and Y silencing maintenance during pachytene stage, thus we hypothesized that an impairment in SETX localization during pachytene should especially impair the X and Y chromosomes.

1. As a general comment to the discussion section, I think authors could extend into some specific ideas or speculations. It is shocking that sex chromosome-linked genes are able to escape silencing without dismantling the complex (almost complete) MSCI response in the Topbp1 mutant (although perhaps this is not so surprising considering the high number of escapees reported in the inactivated X chromosome in female somatic cells).

How to explain this paradox? One possibility (which would make a real breakthrough) is that the expression of sex chromosome-linked genes represents a regulated response to meiotic defects, and not just an unfortunate consequence of a defective MSCI. Thus, MSCI might be somehow irrelevant to prevent the execution of this sex chromosome-based program to stop meiosis progression when needed. The fact that this regulated activation was never proposed is perhaps due to the fact that most of the meiosis mutants characterized so far are unable to reach the stage at which MSCI is properly

*established, which is the most remarkable difference with the Topbp1 mutant studied here.*

*Although naïve, the critical point for the activation of this sex chromosome-based program seems to depend simply on the transcription of Zfy1 and Zfy2 (encoding for transcription factors). The signaling cascades up and downstream these genes are the real mystery, awaiting further studies.*

We thank the very interesting point raised by the reviewer. Our interpretation of the data is that X and Y silencing being a dynamic process requires an initiation step and a maintenance step driven/controlled by the DDR machinery, and that Topbp1B5/B5 shows a grossly normal initiation of X and Y silencing but fails on maintain MSCI. Moreover, the expression of Zfy1 and Zfy2 have been previously demonstrated as enough to trigger cell death (Royo et al., 2010; Vernet et al., 2016), and Topbp1B5/B5 cells show increased expression of these genes. However, we do not exclude the very interesting possibility, raised by the reviewer, that the expression of XY-linked genes represents a regulated response to meiotic defects to stop meiosis progression, leading to the cell death observed in Topbp1B5/B5, which makes the Topbp1B5/B5 an unique model for these studies as most of the previous meiosis mutants are unable to reach the stage at which MSCI is properly established. We add discussion about this exciting point in lines 513-522.

*1. Scale bars are impossible to read in Figures 1I and J, and are missing in all the other image figures. Please, correct.*

We have addressed this in the new Figure 1. For figures displaying meiotic spreads, adding a scale bar is not a common practice in the field as these cells are swollen while being prepared.

*1. Line 828. Since Paula Cohen is an author of the manuscript, it seems weird to acknowledge herself in this section.*

Corrected.

## References

- Adams SR, Maezawa S, Alavattam KG, Abe H, Sakashita A, Shroder M, Broering TJ, Sroga Rios J, Thomas MA, Lin X, Price CM, Barski A, Andreassen PR, Namekawa SH. 2018. RNF8 and SCML2 cooperate to regulate ubiquitination and H3K27 acetylation for escape gene activation on the sex chromosomes. *PLoS Genet* 14. doi:10.1371/journal.pgen.1007233
- Bigot N, Day M, Baldock RA, Watts FZ, Oliver AW, Pearl LH. 2019. Phosphorylation-mediated interactions with topbp1 couple 53bp1 and 9-1-1 to control the g1 DNA damage checkpoint. *Elife* 8:1–28.
- Cescutti R, Negrini S, Kohzaki M, Halazonetis TD. 2010. TopBP1 functions with 53BP1 in the G1 DNA damage checkpoint. *EMBO J* 29:3723–3732.
- Chen Y, Zheng Y, Gao Y, Lin Z, Yang S, Wang T, Wang Q, Xie N, Hua R, Liu M, Sha J, Griswold MD, Li J, Tang F, Tong M-H. 2018. Single-cell RNA-seq uncovers dynamic processes and critical regulators in mouse spermatogenesis. *Cell Res* 28:879–896.
- Hirota T, Blakeley P, Sangrithi MN, Mahadevaiah SK, Encheva V, Snijders AP, ElInati E, Ojarikre OA, de Rooij DG, Niakan KK, Turner JMA. 2018. SETDB1 Links the Meiotic DNA Damage Response to Sex Chromosome Silencing in Mice. *Dev Cell* 47:645-659.e6.



Ichijima Y, Ichijima M, Lou Z, Nussenzweig A, Daniel Camerini-Otero R, Chen J, Andreassen PR, Namekawa SH. 2011. MDC1 directs chromosome-wide silencing of the sex chromosomes in male germ cells. *Genes and Development* 25:959–971.

Lau X, Munusamy P, Ng MJ, Sangrithi M. 2020. Single-Cell RNA Sequencing of the Cynomolgus Macaque Testis Reveals Conserved Transcriptional Profiles during Mammalian Spermatogenesis. *Dev Cell* 54:548–566.e7.

Liu Y, Cussiol JR, Dibitetto D, Sims JR, Twayana S, Weiss RS, Freire R, Marini F, Pellicoli A, Smolka MB. 2017. TOPBP1Dpb11 plays a conserved role in homologous recombination DNA repair through the coordinated recruitment of 53BP1Rad9. *J Cell Biol* 216:623–639.

Modzelewski AJ, Holmes RJ, Hilz S, Grimson A, Cohen PE. 2012. AGO4 regulates entry into meiosis and influences silencing of sex chromosomes in the male mouse germline. *Dev Cell* 23:251–264. Royo H, Polikiewicz G, Mahadevaiah SK, Prosser H, Mitchell M, Bradley A, De Rooij DG, Burgoyne PS, Turner JMA. 2010. Evidence that meiotic sex chromosome inactivation is essential for male fertility. *Curr Biol* 20:2117–2123.

Sims JR, Faça VM, Pereira C, Ascensão C, Comstock W, Badar J, Arroyo-Martinez GA, Freire R, Cohen PE, Weiss RS, Smolka MB. 2022. Phosphoproteomics of ATR signaling in mouse testes. *Elife*

1. doi:10.7554/eLife.68648

Vernet N, Mahadevaiah SK, de Rooij DG, Burgoyne PS, Ellis PJI. 2016. Zfy genes are required for efficient meiotic sex chromosome inactivation (MSCI) in spermatocytes. *Hum Mol Genet* 25:5300–5310.

Ward IM, Minn K, van Deursen J, Chen J. 2003. p53 Binding protein 53BP1 is required for DNA damage responses and tumor suppression in mice. *Mol Cell Biol* 23:2556–2563.

Yeo AJ, Becherel OJ, Luff JE, Graham ME, Richard D, Lavin MF. 2015. Senataxin controls meiotic silencing through ATR activation and chromatin remodeling. *Cell Discovery* 1. doi:10.1038/celldisc.2015.25